



HAL
open science

The TROY project: III. Exploring co-orbitals around low-mass stars

O. Balsalobre-Ruza, J. Lillo-Box, D. Barrado, A. Correia, J. Faria, P. Figueira, A. Leleu, P. Robutel, N. Santos, E. Herrero-Cisneros

► **To cite this version:**

O. Balsalobre-Ruza, J. Lillo-Box, D. Barrado, A. Correia, J. Faria, et al.. The TROY project: III. Exploring co-orbitals around low-mass stars. *Astronomy and Astrophysics - A&A*, 2024, 689, pp.A53. 10.1051/0004-6361/202450717 . hal-04781751

HAL Id: hal-04781751

<https://hal.science/hal-04781751v1>

Submitted on 14 Nov 2024

HAL is a multi-disciplinary open access archive for the deposit and dissemination of scientific research documents, whether they are published or not. The documents may come from teaching and research institutions in France or abroad, or from public or private research centers.









L'archive ouverte pluridisciplinaire **HAL**, est destinée au dépôt et à la diffusion de documents scientifiques de niveau recherche, publiés ou non, émanant des établissements d'enseignement et de recherche français ou étrangers, des laboratoires publics ou privés.



Distributed under a Creative Commons Attribution 4.0 International License

The *TROY* project

III. Exploring co-orbitals around low-mass stars[★]

O. Balsalobre-Ruza¹ , J. Lillo-Box¹ , D. Barrado¹ , A. C. M. Correia^{2,3} , J. P. Faria⁴ , P. Figuera^{4,5} ,
A. Leleu⁴, P. Robutel³, N. Santos⁵ , and E. Herrero-Cisneros⁶ 

¹ Centro de Astrobiología (CAB), CSIC-INTA, Camino Bajo del Castillo s/n, 28692 Villanueva de la Cañada, Madrid, Spain
e-mail: obalsalobre@cab.inta-csic.es

² CFisUC, Departamento de Física, Universidade de Coimbra, 3004-516 Coimbra, Portugal

³ IMCCE, UMR8028 CNRS, Observatoire de Paris, PSL Université, 77 Av. Denfert-Rochereau, 75014 Paris, France

⁴ Observatoire Astronomique de l'Université de Genève, Chemin Pegasi 51b, 1290 Versoix, Switzerland

⁵ Instituto de Astrofísica e Ciências do Espaço, Universidade do Porto, CAUP, Rua das Estrelas, 4150-762 Porto, Portugal

⁶ Centro de Astrobiología (CAB), CSIC-INTA, Crta. Ajalvir km 4, 28850 Torrejón de Ardoz, Madrid, Spain

Received 14 May 2024 / Accepted 13 June 2024

ABSTRACT

Context. Co-orbital objects, also known as trojans, are frequently found in simulations of planetary system formation. In these configurations, a planet shares its orbit with other massive bodies. It is still unclear why there have not been any co-orbitals discovered thus far in exoplanetary systems (extrojan) or even pairs of planets found in such a 1:1 mean motion resonance. Reconciling observations and theory is an open subject in the field.

Aims. The main objective of the *TROY* project is to conduct an exhaustive search for extrojan using diverse observational techniques. In this work, we analyze the radial velocity time series informed by transits, focusing the search around low-mass stars.

Methods. We employed the α -test method on confirmed planets searching for shifts between spectral and photometric mid-transit times. This technique is sensitive to mass imbalances within the planetary orbit, allowing us to identify non-negligible co-orbital masses.

Results. Among the 95 transiting planets examined, we find one robust extrojan candidate with a significant $3\text{-}\sigma$ detection. Additionally, 25 exoplanets show compatibility with the presence of extrojan companions at a $1\text{-}\sigma$ level, requiring further observations to better constrain their presence. For two of those weak candidates, we find dimmings in their light curves within the predicted Lagrangian region. We established upper limits on the co-orbital masses for either the candidates and null detections.

Conclusions. Our analysis reveals that current high-resolution spectrographs effectively rule out co-orbitals more massive than Saturn around low-mass stars. This work points out to dozens of targets that have the potential to better constraint their extrojan upper mass limit with dedicated radial velocity observations. We also explored the potential of observing the secondary eclipses of the confirmed exoplanets in our sample to enhance the extrojan search, ultimately leading to a more accurate estimation of the occurrence rate of extrojans.

Key words. techniques: photometric – techniques: radial velocities – minor planets, asteroids: general – planets and satellites: detection – stars: low-mass

1. Introduction

Co-orbital configurations abound in the Solar System, where two massive bodies share their orbital path around the star. However, their detection beyond our system remains elusive. Two different mechanisms have been proposed to explain their formation, which are also expected to apply to exoplanetary systems: 1) in situ from the same material as protoplanets (e.g., Beaugé et al. 2007) or 2) via resonant captures at more advanced stages (e.g., Namouni & Morais 2018). Recent ALMA observations of three protoplanetary disks may be the first observational hints in favor of their in situ assembly, since they exhibit substructures that could be interpreted as an accumulation of material within the L_4 & L_5 Lagrangian points of forming planets. In HD 163296 and LkCa 15, it has been found asymmetric emissions with shapes

that are reminiscent of the dust traps that appear in the process of trojan formation, as seen in hydrodynamical simulations (Isella et al. 2018; Long et al. 2022). An equivalent unresolved emission was found also in PDS 70 promisingly matching the L_5 region of the protoplanet PDS 70 b (Balsalobre-Ruza et al. 2023).

As posited by Laughlin & Chambers (2002), two co-orbiting similar-mass planets can be stable in the long term. Such stability remains possible as long as the total mass of the planet and the trojan does not surpass 3.7% of their host star mass (i.e., $[m_p + m_t]/M_\star < 1/27$). This constraint allows for multiple co-orbital configurations to remain longstanding, including pairs of equal-mass planets. Although this exotic configuration is absent in the Solar System, its theoretically hypothesized stability encourages the detectability of extrojan pairs for the first time. Such co-orbital systems could be accessible using current instrumentation, even from the ground (e.g., Ford & Gaudi 2006; Haghhighipour et al. 2013; Hippke & Angerhausen 2015).

* Full Table B.2 is available at the CDS via anonymous ftp to cdsarc.cds.unistra.fr (130.79.128.5) or via <https://cdsarc.cds.unistra.fr/viz-bin/cat/J/A+A/689/A53>

The absence of detections in exotrojan studies so far may be attributed to two non-exclusive reasons: (i) co-orbital configurations might get disrupted earlier than theoretically predicted and (ii) observational biases, as degeneracies with simpler configurations for the observed signals (see e.g., [Giuppone et al. 2012](#); [Goździewski & Konacki 2006](#)) or the existence of transit timing variations (hereafter TTVs, e.g., [García-Melendo & López-Morales 2011](#); [Leleu et al. 2021b](#)) can prevent their detection. Dedicated studies are therefore needed to ascertain the presence of the 1:1 mean motion resonance (MMR) in planetary system. This is the purpose of the *TROY* project¹, which this work builds on, following [Lillo-Box et al. \(2018a,b\)](#). Here, we extend the search for trojans accompanying confirmed exoplanets through a combination of radial velocities (RVs) and transit information. Former studies of these series were aimed at initiating searches in systems where the expected signal of a co-orbital pair is maximized and therefore easily distinguishable from a single-planet configuration. That preliminary search allowed us to estimate the upper limit of the occurrence of trojans for short-period ($P < 5$ d) giant planets. Also, it yielded nine candidates, although none proved significant. Here, we did not restrict the search to hot Jupiters, but we included any type of exoplanet orbiting low-mass stars (in the M and late-K spectral type regime). Despite hot Jupiters being easier targets from a detectability perspective, they are not necessarily the most suitable systems to host trojans due to the tidal forces of the star disrupting these configurations ([Couturier et al. 2021](#); [Dobrovolskis & Lissauer 2022](#)).

In Sect. 2, we explain the selection process for the new sample comprising 84 low-mass stars. Section 3 outlines the method used to test the co-orbital scenario, namely, the so-called α -test. Section 4 presents the results, followed by a discussion in Sect. 5. The conclusions are provided in Sect. 6.

2. Target selection and data retrieval

Our sample selection is based on the NASA Exoplanet Archive (NEA) planetary systems table² ([Akeson et al. 2013](#)) in November 2023, which encompasses all the “confirmed” planets to date. We applied the following criteria to select the sample.

First, the stellar effective temperature was set to be below 4650 K to focus the survey on low-mass stars. This corresponds with spectral types later than K4 V. Then, the system hosting up to two planets to avoid highly complex RV signals. This would reduce the number of free parameters and, consequently, the degree of degeneracy. Next, at least one of the planets must transit the star. This requirement relies on the methodology, as it exclusively applies to transiting planets. Finally, the transiting planets also have to be detected by radial velocities, since our method is based on the analysis of publicly available RVs.

A total of 88 systems fulfill these criteria. Seven of them were excluded for various reasons. According to the discovery papers, GJ 1132 and TOI 1266 require three Keplerians to reproduce the RV signal ([Bonfils et al. 2018](#); [Cloutier et al. 2024](#)), indicating an additional planet candidate not listed in the NEA table. Kepler-16 is a binary star hosting a circumbinary planet that transits both stars ([Triaud et al. 2022](#)); hence, the detection method we used cannot be applied to this system (see Sect. 3). Kepler-91 is ascending the red giant branch and therefore is out of our regime of study (but see [Lillo-Box et al. 2014](#), where the presence of a

Trojan for this system is studied). Also noteworthy are the cases of LHS 1815, TOI-2136, and Wendelstein-2, which have insufficient RV observations; therefore, the planet was undetectable and the candidate was only validated ([Gan et al. 2020](#); [Beard et al. 2022a](#); [Obermeier et al. 2020](#)). These cases highlight the need for establishing a protocol that standardizes the requirements for considering a planet as confirmed ([Lillo-Box et al., in prep.](#)), which would highly facilitate archival works.

Finally, we added K2-199, TOI-532, and TOI-1801 as these targets meet our constraints but at the time of writing are not yet included as detected by RV variations in the NEA. In summary, our final sample is composed of 84 systems hosting a total of 95 transiting planets. We note that our sample contains some targets previously analyzed in [Lillo-Box et al. \(2018a,b\)](#). However, we decided to preserve them for homogeneity. In some cases, new RV measurements are available, and we incorporated some changes in the analysis (e.g., we set the eccentricity to be below 0.1, and we fixed the orbital period and the mid-transit time to the photometric according to the prescription in [Leleu et al. 2017](#); see Sect. 3).

All the RV datasets used in this work have been obtained from the literature. In Table B.1, we summarize them, including the number of measurements (out of transit, see Sect. 3) and instruments, the time span, and the reference we retrieved the data from. The RV datasets used for all the targets can be found in Table B.2. In Fig. 1, we illustrate the final sample. On the left, the stellar mass distribution showcases the covered spectral domain (spectral types are based on [Cifuentes et al. 2020](#), valid for main-sequence low-mass stars). On the right panel, we show the period-mass diagram for all confirmed NEA exoplanets (excluding the ones detected by the imaging technique), where the color code indicates the stellar effective temperature and the sizes offer information on the number of RV measurements available for our analysis.

We conducted an examination of potential selection biases within our sample: (i) only 10% of systems with confirmed planets fall within our target spectral domain (earlier than K4). To our knowledge, no works have shown co-orbital preference for any spectral type over another. However, [Leleu et al. \(2019\)](#) and [Coleman et al. \(2019\)](#) show that multiple planetary systems in resonant chains tend to retain the co-orbital configurations, two factors that could be more common around low-mass stars systems (e.g., Trappist-1); (ii) three systems (L 98-59, [Demangeon et al. 2021](#); TOI-178, [Leleu et al. 2021a](#); TOI-500, [Serrano et al. 2022](#)) lie outside our sample due to hosting more than two confirmed planets; this means our study comprises 97% of low-mass star planetary systems and, therefore, no bias is anticipated from this constraint. We note that even if these stars are expected to host numerous planets ([Kunimoto & Matthews 2020](#)), they may remain undetectable with current instrumentation; (iii) like any statistical study focusing on transiting planets, our sample is biased towards large-radius planets in edge-on architectures. The former bias is compensated by the fact that low-mass stars host lighter and smaller planets and the signal of such planets in both techniques (RVs and transits) are also enhanced in this spectral domain. Specifically, 51% of our observed planets are below a Neptune mass, 34% fall between Neptune and Jupiter masses, and 15% exceed the Jupiter mass. No effect is therefore expected in our study apart from the difficulty on studying the RV signals of the less massive planets. Regarding the edge-on orientation, as there are not obvious co-orbital transits in their light curves, our sample is biased to non-coplanar co-orbital configurations, or to small radii exotrojans; (iv) the spectral-type domain and the nature of the detection methods also contribute to the fact

¹ www.troy-project.com

² <https://exoplanetarchive.ipac.caltech.edu/cgi-bin/TblView/nph-tblView?app=ExoTbls&config=PS>

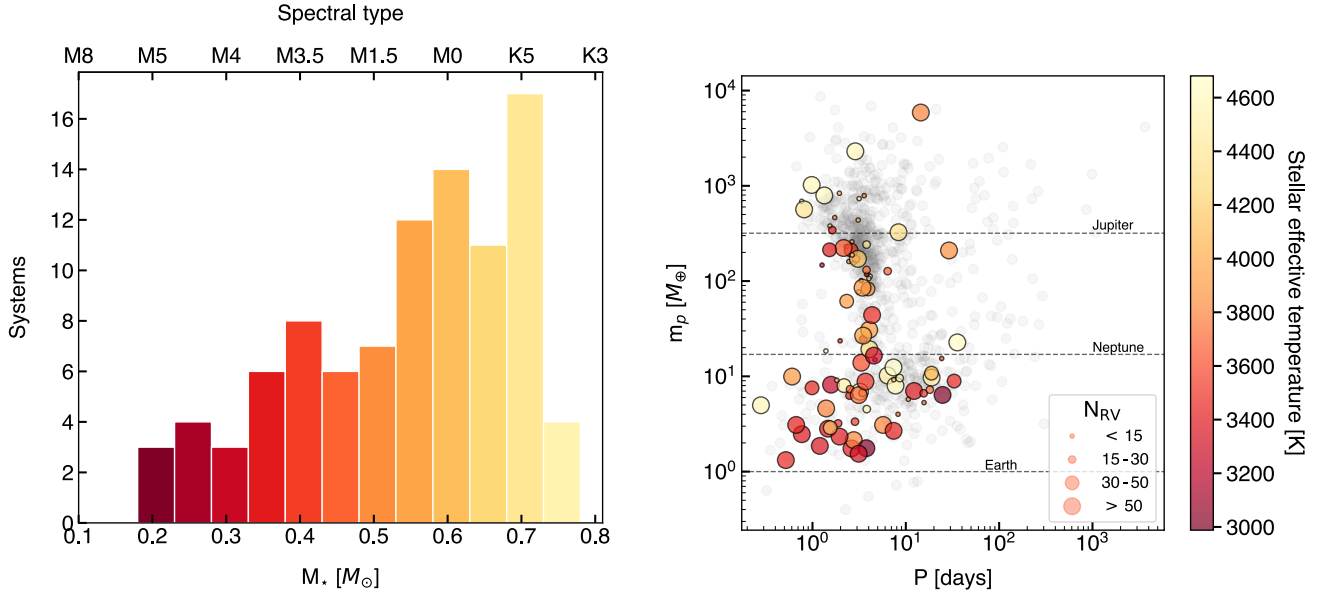


Fig. 1. Sample of the study. *Left:* distribution of the stellar spectral type (color coded by the effective temperature). *Right:* period-mass diagram for all confirmed planets excluding those discovered by the imaging technique. Colored symbols correspond to the targets from our sample selected as explained in Sect. 2, where the color code indicates the effective temperature of the host star. The size of the colored dots informs on the number of RV measurements available for this work as indicated in the legend. The three horizontal lines show the masses of Jupiter, Neptune, and Earth for reference.

that the majority of planets in our sample have short periods (85% of them are below 10 days). Tidal interactions for those planets could have an impact preventing the long-term co-orbital stability (Correia et al. 2020) and this factor is even more critical around low-mass stars (Couturier et al. 2021). Therefore, for our sample we would expect to only find exotrojan evidence for the youngest systems or with longer orbital periods.

3. Methodology

A configuration with a single planet and a pair of co-orbitals can be identified using RV time series. Assuming a long time baseline and high cadence for the RV measurements, it is possible to detect the modulation in the main-planet signal as its trojan librates (see e.g., Leleu et al. 2015). Nonetheless, when the libration of the trojan is negligible as in the case of usual RV monitoring campaigns (spanning few months and with relatively sparse data), the key factor to reveal the presence of a co-orbital configuration is having information about the time of conjunction of the main planet (i.e., T_0). Even if the RV signal is compatible with a single planet scenario, the inferred transiting time from this technique would correspond with that of the centre of mass of the co-orbitals (Ford & Gaudi 2006). Therefore, if there is an imbalance in the masses of the Lagrangian regions, there would be a shift between the photometric and the RV inferred T_0 . We note that this is the case as far as an asymmetry exists between the Lagrangian points L_4 and L_5 : (i) a single trojan leading or trailing the main planet, (ii) two trojans each in its own tadpole (i.e., configuration in which the trojan librates around L_4 or L_5) region but unbalanced in mass, or (iii) a trojan in a horseshoe (i.e., the trojan travels from L_4 to L_5 going through L_3 as well) orbit but with a libration period larger than the observation time span. Conversely, this method would be “blind” to equal mass trojans located in L_4 and L_5 regions. We note that all of these scenarios are equivalent when a swarm of asteroids replaces the compact body.

Leleu et al. (2017) generalized the RV equation as a function of time (t) for this method as follows:

$$\Delta v(t) = K [(\alpha - 2c) \cos nt - \sin nt + c \cos 2nt + d \sin 2nt], \quad (1)$$

with K as the RV semi-amplitude, and n the mean orbital frequency. Parameters c and d depend on the orbital eccentricity (e) and the argument of periastron (ω) as $c = e \cos \omega$, and $d = e \sin \omega$. The α -parameter is the one that holds the trojan information. To the first order in eccentricity, it takes the form:

$$\alpha \approx m_t/m_p \sin \zeta, \quad (2)$$

where m_t/m_p is the trojan-planet mass ratio, and ζ is the resonant angle that locates the trojan within the orbit (e.g., $60^\circ/-60^\circ$ for L_4/L_5). Thus, a significantly non-zero value of this parameter would suggest the presence of a massive trojan. As in Lillo-Box et al. (2018a), we follow the α -test approach to search for trojans accompanying confirmed planets (i.e., transiting planets which mass has been measured through RVs). We note that Eq. (1) does not account for the Rossiter-McLaughlin (R-M) effect and for this reason, we removed the RV measurements taken during the transit.

The model and the amount of parameters that need to be explored depend on the number of detected planets (N_{pla}), transiting planets (N_{tra}), and instruments used to gather the measurements (N_{ins}). By construction, our sample is only composed of systems with one or two planets, and at least one of them must transit. The RV dataset of each transiting planet was modeled using Eq. (1), whose free parameters are the RV semi-amplitude (K), the orbital architecture (c and d), and the α metric. The key to comparing the spectral and photometric mid-transit times relies on fixing the mean motion ($nt = 2\pi[t - T_0]/P$), using the parameters inferred from the transits (collected in Table B.1). We note that for systems composed of two transiting planets, we searched for co-orbitals in both orbits simultaneously, fixing both periods and mid-transit times. Some of the literature values for

the T_0 parameter were inferred in the corresponding works from a joint analysis considering also the RV data. Nonetheless, there is no conflict with this method since the T_0 parameter is mainly derived from the transiting signal as required (the RV dataset is typically not able to constrain it as precisely as the transits, on the order of minutes). Meanwhile, the RV signal of not-transiting planets was modeled with a classic Keplerian³, whose parameters are K , c , d , T_0 , and the orbital period, P . Finally, we added an offset and a jitter per instrument to account for instrumental dependencies and unaccounted systematics, respectively. Thus, we ended up with a total of $5N_{\text{pla}} - N_{\text{tra}} + 2N_{\text{ins}}$ parameters for the modeling.

If the activity of a star is affecting the RV time series, we included a Gaussian process (GP) to account for it. This decision was made when the rotational period (P_{rot}) is present in the generalized Lomb-Scargle (GLS) periodogram of at least one spectral activity indicator such as the full width half maximum (FWHM) of the cross correlation function (CCF), the differential line width (dLW), or the H_α emission line, among others. In some occasions, the RV measurements are also correlated with the activity indicators showing that the same signal is present, and in the most obvious cases, the high RV scatter caused by the activity hinders the detection of the planetary signal. In all the cases, the GP was informed based on an activity proxy, which was chosen for being the indicator that most clearly shows P_{rot} (see Appendix A for the details on the particular cases). We implemented the GP using the george python package (Ambikasaran et al. 2015) opting for a quasi-periodic kernel (QP, e.g., Faria et al. 2016) of the form:

$$\Sigma_{ij} = \eta_1^2 \exp \left[-\frac{(t_i - t_j)^2}{2\eta_2^2} - \frac{2\sin^2 \left(\frac{\pi(t_i - t_j)}{\eta_3} \right)}{\eta_4^2} \right]. \quad (3)$$

Hence, the GP implementation introduces increments into the number of parameters in $5 + 2N_{\text{ins}}$. The proxy and the RV signal need an independent amplitude ($\eta_{1,\text{prx}}$ and $\eta_{1,\text{RV}}$), there is an aperiodic timescale (η_2), a correlation period (η_3), and a periodic scale (η_4). Additionally, the activity proxy requires a constant (C) and a jitter per instrument. We note that we only consider an amplitude $\eta_{1,\text{prx}}$ and $\eta_{1,\text{RV}}$ shared for all instruments. Therefore, it represents an average amplitude of the activity signal, which might not be ideal specially when the instruments cover different wavelength ranges.

To sample the posterior distribution of the model parameters we employ the Markov chain Monte Carlo (MCMC) affine invariant ensemble sampler emcee (Foreman-Mackey et al. 2013). We use five (ten when adding a GP) times the number of parameters for the walkers and between 6×10^4 and 2×10^5 steps, following a second run starting the new chains around the maximum a posteriori set of parameters and with half of the steps to speed up the convergence. The number of steps is adapted to ensure that the length of the chains is at least 50 times the autocorrelation time per parameter.

In Table 1, we show the priors adopted in the analysis. For most of the priors, we opt to use uniform distributions in order to be uninformative. In the case of the RV semi-amplitude (K), we choose the scatter of the RV ($\text{RV}_{\text{scatter}} = \text{RV}_{\text{max}} - \text{RV}_{\text{min}}$) to be the upper limit of the uniform distribution. The selection of this prior has proven to be good enough as our posteriors on this parameter converge to values below half of the parameter space (i.e., $\text{RV}_{\text{scatter}}/2$). We choose equivalent priors for the

Table 1. Prior distributions.

Parameter	Prior	Units
K	$\mathcal{U}(0, \text{RV}_{\text{scatter}})$	m s^{-1}
c	$\mathcal{U}(-1, 1)$ or $\mathcal{G}_t(c_{\text{occ}}, \Delta c_{\text{occ}})$	
d	$\mathcal{U}(-1, 1)$ or $\mathcal{G}_t(d_{\text{occ}}, \Delta d_{\text{occ}})$	
e_{tra}	$\mathcal{U}(0, 0.1)$	
P_{ntr}	$\mathcal{G}_t(P, \Delta P)$	d
T_0, ntr	$\mathcal{G}_t(T_0, \Delta T_0)$	d
α	$\mathcal{U}(-1, 1)$	
jitter	$\mathcal{U}(0, \text{RV}_{\text{scatter}}/4)$	m s^{-1}
offset	$\mathcal{U}(\text{RV}_{\text{min}}, \text{RV}_{\text{max}})$	m s^{-1}
GP hyperparameters		
C	$\mathcal{U}(\text{Proxy}_{\text{min}}, \text{Proxy}_{\text{max}})$	Proxy units
jitter _{prx}	$\mathcal{U}(0, \text{Proxy}_{\text{scatter}}/4)$	Proxy units
$\eta_{1,\text{prx}}$	$\mathcal{U}(0, \text{Proxy}_{\text{scatter}})$	Proxy units
$\eta_{1,\text{RV}}$	$\mathcal{U}(0, \text{RV}_{\text{scatter}})$	m s^{-1}
η_2	$\mathcal{U}(2P_{\text{rot}}, 1000)$	d
η_3	$\mathcal{G}_t(P_{\text{rot}}, \Delta P_{\text{rot}})$	d
η_4	$\mathcal{U}(0, 5)$	

Notes. The subscripts identify parameters only applicable for transiting (tra), and not transiting (ntr) planets, and (occ) are for the values inferred from occultations.

amplitudes of the GP ($\eta_{1,\text{prx}}$ and $\eta_{1,\text{RV}}$). We did constrain c and d with a normal distribution for the planets with detected secondary eclipses by computing their values as Eqs. (33) and (34) from Winn (2010) and changing their sign to transform into the planet frame (see Table B.3). These are the most reliable candidates since α is degenerated to some extent with the orbital architecture (e), being the secondary transit the only means to disentangle them. When no secondary eclipse is available, we need to work under the assumption of low-eccentricity orbits ($e < 0.1$) to be able to apply our methodology since Eq. (1) is only valid for eccentricities below this value. Hence, it is important to note that our results are subjected to this scenario. When the orbital period of the planets (either transiting or not) are below 10 days, we do an additional test setting them to circular orbits ($e = 0$, as based on the tidal circularization criterion, for example, Jackson et al. 2008). In the case of systems where one of the planets does not transit, we used normal distributions for the Priors of P and T_0 using the data from the bibliography tabulated in Table B.1. The priors for the GP hyperparameters are normal distributions based on literature posteriors if a QP GP has already been implemented for that particular system, or are those shown in Table 1 otherwise.

4. Results

There are 95 transiting planets from the 84 systems for which we can inspect their α searching for co-orbital signs. We test up to four models per system: the slightly eccentric orbit model (where the eccentricity is either below 0.1 or constrained by the secondary eclipse), the circular orbit model (if $P < 10$ days), and those two models but including a GP if needed (P_{rot} signal present in a spectral indicator). We selected the GP model as the best one (when available) and we decided among the circular and eccentric models by means of the Bayes factor ($\ln \mathcal{Z}$), computed with the bayev code (Díaz et al. 2016). Remarkably, for all of the cases the circular model (simpler) is favored over the eccentric scenario, with $\ln \mathcal{Z} > 3.5$.

³ We use the python module RadVel (Fulton et al. 2018).

Table 2. Target classification.

$\alpha^{(a)}$	Criterion	Group	Members
$\neq 0$	$ \alpha /\sigma_\alpha > 3$	Strong candidate	1
	$1 < \alpha /\sigma_\alpha < 3$	Weak candidate	25
$= 0$	$\sigma_\alpha > 0.15$	Inconclusive	21
	$\sigma_\alpha < 0.15$	Null detection	10
	$\Delta\phi > 0.15$ or $N_{RVs} < 15$	Sparsely sampled	37

Notes. ^(a)Within 68.3% of confidence interval ($1-\sigma$).

We classified the sample into four groups based on the inferred α . The most relevant are the “strong candidates” (SC) and the “null detections” (ND) groups since they provide conclusive results. The SC are the planets with an α value different from zero within a 99.7% confidence interval ($|\alpha|/\sigma_\alpha \geq 3$), therefore being co-orbital detections by the α -test. On the other hand, ND are planets with null α values as far as the uncertainty is below 15% ($\sigma_\alpha < 0.15$), being observationally very expensive to better constrain the presence of an hypothetical co-orbital and, therefore, we rule them out as candidates. In between, we distinguish the “weak candidates” (WC), and the “inconclusive candidates” (INC). For both of them, there is a large uncertainty in terms of their α values that would be required to gather more (or more precise) data until reaching conclusive results. Nonetheless, for the WC, the α differs from zero within $1-\sigma$ to $3-\sigma$, hinting at the presence of trojans as promising targets that should continue to be monitored. In Table 2, there is a summary for this classification criterion. We note that the sum of the members is 94 since one of the targets (GJ 3090 b) is rejected for being out of the methodology domain (see Appendix A for more details).

A large number of transiting planets in the sample (37, being the 40%) have a poor coverage in the orbital phase space. The criterion we adopted to tag a system as “sparsely sampled” (SS) is that each orbital phase bin of 0.15 contains less than one measurement (i.e., $\Delta\phi > 0.15$, being $\Delta\phi$ the orbital phase difference between consecutive data points), or the total number of data points is below 15 (i.e., $N_{RVs} < 15$). We included these targets in the analysis for completeness and also because they are relevant targets with respect to expanding the sample in the near future. Nonetheless, we did not classify them in the groups mentioned above and we do not consider them for the discussion. The resulting α for all the tested models can be found in Table B.4 and are displayed in Fig. C.1 for the grouped targets.

Only one planet stands out as SC: GJ 3470 b. This is a hot Neptune of around $14 M_\oplus$ in a 3.3-days orbit that has been intensively explored. There is no evidence for the existence of a second planet orbiting the M-dwarf, including no significant TTVs (below 500 s, Awiphan et al. 2016). The outcome of the analysis corresponds with a co-orbital detection at a $3-\sigma$ level ($\alpha = -0.16 \pm 0.05$). GJ 3470 b is a very strong candidate not only by its significance, but also because the orbital architecture of this planet is constrained by the secondary eclipse observed with *Spitzer*. Though, we note that the uncertainty in d (see Table B.3) is wide and the posterior tends to an eccentric orbit ($e \sim 0.1$) hence a better eccentricity constraint would be valuable. For more information on the analysis, we refer to Appendix A.

Remarkably, both transiting planets orbiting TOI-1130 have not null α values with a higher significance ($\sim 4-$ and $12-\sigma$) than GJ 3470. Nonetheless, we downgrade them to WCs, since

Korth et al. (2023) reported strong TTVs in both planets (more than 2 h of amplitude for planet b) by using TESS and ground-based photometry. As Leleu et al. (2017) warn, planets with coupled orbital periods in 2:1 MMR (as in the case of TOI-1130, with 4.1 and 8.4 days) can induce false positives due to their possible TTVs. Nonetheless, the time span of the RV dataset we use (62 days) covers around 15 orbits of the inner planet, which should mitigate the TTV impact in the inferred α . For this reason, we either rule out this target as a candidate. Other systems near 2:1 MMR are present in the sample: HD 260655 (with periods of 2.8 and 5.7 days), K2-199 (3.2 and 7.4 days), TOI-776 (8.2 and 15.7 days), and TOI-836 (3.8 and 8.6 days). All of these targets have at least one not null α , yet TOI-836 c is the only planet that exhibits TTVs in the order of 20 min (Luque et al. 2021, 2022; Hawthorn et al. 2023). We recall, as mentioned above (Sect. 2), that resonant chains are expected to help preserving the co-orbital stability.

The cases of GJ 143 b, and HIP 65 A b are also noteworthy. The former planet orbits a presumably active star as its rotational period appears in the activity indicators. Nonetheless, when including a GP the uncertainty in α is greatly increased in almost a factor of five, taking this target from the WC group to the INC. For HIP 65 A b, the result hardly depends on the eccentricity being a WC for the slightly eccentric model and ND for the circular. Since this planet has a grazing transit ($b \sim 1$ according with Nielsen et al. 2020), breaking the degeneracy through the eclipse might not be possible.

It is interesting to note that HAT-P-20 b and WASP-43 b have an extraordinary low uncertainty, namely: 0.2 and 0.5% of the α parameter space. Both of them are favoured due to the fact that they are hot Jupiters that induce a big RV semi amplitude into their stars (~ 1240 and 555 m s^{-1}), by the determination of the eccentricity by the occultation and also by the high quality of their observations (using HARPS and ESPRESSO spectrographs). In the case of WASP 43 b, the majority of the measurements were taken around the transit, which is also likely to favour an accurate mid-transit time being obtained through the RVs, as an advantage for our methodology. This was also found for WASP-80 b (see Appendix A).

5. Discussion

5.1. Co-orbital mass

In order to estimate the trojan mass, we use Eq. (2) by fixing $\zeta = \pm 60^\circ$. These resonant angles correspond to tadpole orbits in which the co-orbitals librate around L_4 or L_5 , the most common configurations based on numerical simulations (e.g., Leleu et al. 2019). We take the percentiles at the 95.45% confidence interval (2.3 and 97.7) of the α posterior distribution inferred for the best model per system (see Sect. 4, and specified in Table B.4) to compute the upper limit on the trojan mass. We tabulate those masses in Table B.4. For the only SC in our sample (GJ 3470 b), we obtain the predicted posterior distribution of the trojan mass in L_5 by taking the whole distribution of α , resulting in $m_t = 2.6 \pm 0.7 M_\oplus$.

Figure 2 graphs the maximum of the co-orbital mass upper limit (between L_4 and L_5) as a function of the planetary mass. In this diagram, we find that for 34 of the planets (59%), the upper limit of the hypothetical trojans is above half of the mass of the main planet (within the light orange region). We would expect this area to be empty based on theoretical studies (Pierens & Raymond 2014); indeed, most of those targets correspond to the WC and INC groups, underscoring the fact that

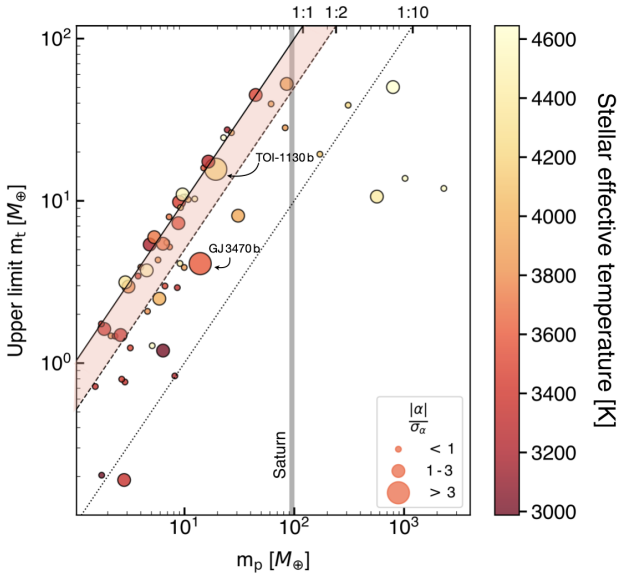


Fig. 2. Upper limit of the trojan mass versus the mass of the confirmed planet. Black lines indicate equal mass ratios (solid line) along with the 1:2 (dashed) and 1:10 relations (dotted). The vertical grey solid line indicates the mass of Saturn. The light orange region corresponds to trojan masses higher than theoretically expected (between 1:1 and 1:2). The size of the symbols informs about the significance of the co-orbital candidate as shown in the legend. Color code represents the stellar effective temperature as shown in the color bar.

our current datasets do not constraint the co-orbital presence. On the other hand, only ten targets (17%) have the mass ratio m_t/m_p restricted to be below the 20%. Interestingly, six of those are the only planets in our sample with planetary masses above Saturn ($\sim 100 M_\oplus$). From this observational result based on the available time series and the α -test method, we can infer two conclusions: (i) currently, for planets less massive than Saturn we cannot restrict the presence of trojans; and (ii) there is no observational evidence for the presence of trojans more massive than Saturn around low-mass stars. Notably, some of the less massive planets (e.g., GJ 486 b, LHS 1140 c, and TOI-244 b) have their co-orbital companions restricted in more than the 50%. The reason is that a more exhaustive RV monitoring with outstanding precision was needed for their detection, which shows that it is currently feasible to carry out dedicated searches to efficiently restrict the uncertainties in the α parameter.

In Fig. 3, we show the cumulative lower limit occurrence rate of trojans as a function of their upper mass limits, compared with the distribution of the confirmed main planets. As already discussed, there are no Saturn-mass trojans expected accompanying the giant planets that orbit low-mass stars, which represent 15% of our sample. Less than the 18% of the planets are expected to be accompanied by Neptune-mass trojans, and roughly 80% can have trojans less massive than the Earth. Comparing with the confirmed population of Neptunes (20%) and with planets less massive than the Earth (100%, since such planets remain undetectable to date), we notice again that current RV datasets are unable to give strong constraints to the presence of co-orbitals and, therefore, on the occurrence rate.

5.2. Search for Lagrangian point transits

Under the assumption of (near) circular orbits and (near) coplanarity of the main planet and the potential co-orbital companion,

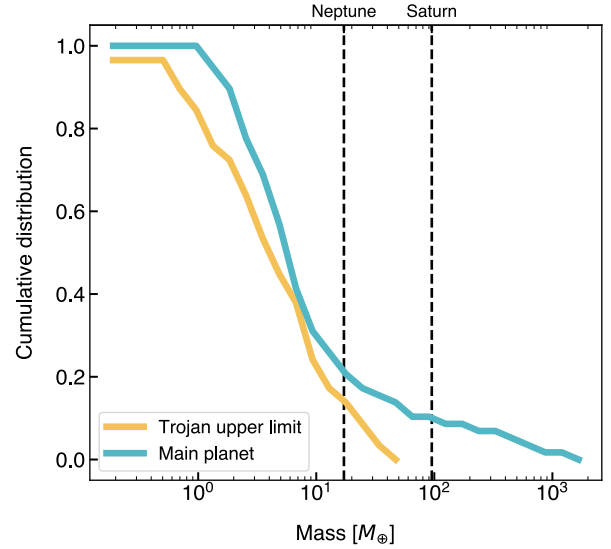


Fig. 3. Occurrence rate of trojans and mass distribution of the main planets.

if the main planet transits its host star from our line of sight, the co-orbital could also do so. Hence, for the cases where we find some hints for the presence of co-orbital bodies (WC sample), it is worth checking the available space-based time series photometry around the Lagrangian regions, seeking for a dimming induced by these (still weak) candidates. It is however relevant to mention that while having near-circular orbits is a requisite to apply our α -test, coplanarity is neither required nor necessary to keep the stability of a co-orbital pair (e.g., [Leleu et al. 2017](#)). Consequently, non-detections within this exercise only constrain the parameter space for the existence of the trojan corresponding to the near-coplanar case, while larger mutual inclinations are still possible.

Our main light curve source is the Transiting Exoplanets Satellite Survey (TESS, [Ricker et al. 2014](#)), but when available, we also retrieved the K2 data ([Borucki et al. 2010](#); [Howell et al. 2014](#)). We use the `lightkurve` ([Lightkurve Collaboration 2018](#)) package to retrieve the processed detrended light curves from these missions. For TESS, we use the SPOC pipeline ([Jenkins et al. 2016](#)) with a 2-min cadence. For K2, we use the K2 pipeline with a 30-min cadence. For each of the planets in the WC list, we retrieved the light curve from all available sectors (TESS) or campaigns (K2). We then performed a detrending using `wotan` ([Hippke et al. 2019](#)). To this end, all transits from any planet in the system are masked. The detrended and normalized light curves are then phase-folded with the planet ephemeris. The zoomed-in light curves around the Lagrangian points L_4 and L_5 for each planet are presented in Fig. C.4, with bin sizes corresponding to 10% (red symbols) and 20% (blue symbols) of the planet's transit duration. On each panel, we mark in color (orange for L_4 and blue for L_5) the Lagrangian point where our α -test has yielded the (weak) candidate. In most cases, the light curves around these regimes show a flat behaviour, with no detectable transits.

In some cases (specially in the K2 data), the light curves are very noisy, potentially due to stellar activity not appropriately removed with our detrending process. However, in some few cases, the light curves seem to show dimmings compatible with the duration and location expected for a co-orbital planet. In particular, this is the case for LHS 1140 b, which shows very

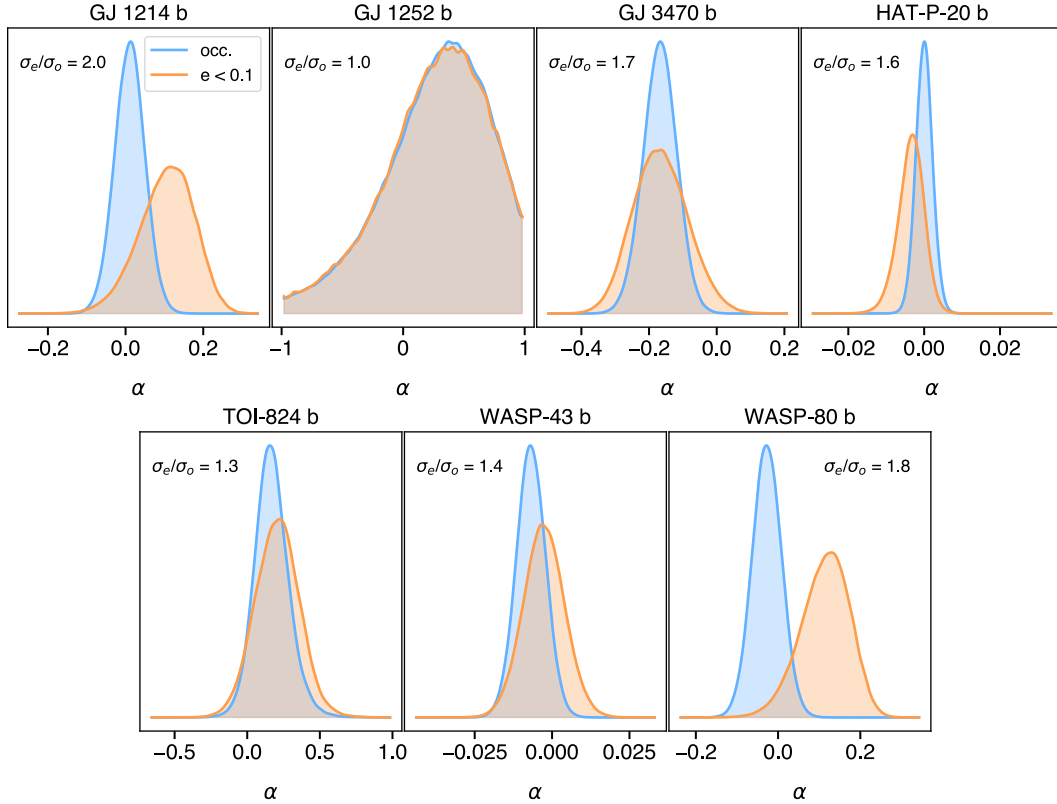


Fig. 4. Comparison of the α posterior distribution when using normal priors for the orbital architecture informed from the occultation (blue) and when using uniform priors with $e < 0.1$ (orange). The improvement in the precision as the ratio of their σ is shown in the upper corner of each chart.

shallow dimmings at both L_4 and L_5 , although still compatible with the noise. Other two interesting cases are TOI-776 b (L_5) and TOI-836 b (L_4). They both show relatively clear dimmings at their corresponding Lagrangian points where the α -test locates the co-orbital candidates. The dimmings would correspond to objects of around $1 R_{\oplus}$. The estimated masses for the trojan candidates given the inferred α values are $2.8 \pm 1.6 M_{\oplus}$ (TOI-776 L_5 b) and $1.9 \pm 0.9 M_{\oplus}$ (TOI-836 L_4 b). The estimated planet radius for such masses using the empirical relations from [Chen & Kipping \(2017\)](#) are $1.44^{+0.78}_{-0.42} R_{\oplus}$ and $1.18^{+0.49}_{-0.25} R_{\oplus}$, respectively. Interestingly, these values match the detected dimmings. Further observations on this system will be critical to provide additional insights towards the confirmation of these candidates. Meanwhile, there are no detectable dimmings for GJ 3470 b. This means that there is no transiting counterpart for the strong trojan candidate with radius larger than $\sim 1 R_{\oplus}$.

5.3. Occultations

Throughout this study, we have emphasized the critical importance of detecting occultations to reliably constrain the planetary eccentricities. This methodology stands as the sole means to resolve the degeneracy between eccentricity and α . Only seven planets within our sample have had their secondary transits measured to our knowledge. In order to visualize the improvement, in Fig. 4, we compare the posterior distribution of their α with the one obtained if no occultation were to be observed (assuming $e < 0.1$). For all the cases (except for GJ 1252 which is part of the SS targets), the precision in the inferred α is increased, being a factor two for GJ 1214. The magnitude is also shifted in some of the cases, being a false candidate in GJ 1214 and WASP 80,

when no occultation is measured. In this section, we focus on assessing the feasibility of detecting more occultations among our target planets.

When the planet is eclipsed by the host star, the received flux is reduced the quantity corresponding to that of the emitted by the planet. Its emission is compound by the thermal radiation and the reflected starlight. The former is only not negligible as compared with the starlight when observing at long wavelengths. Hence, infrared instruments such as *Spitzer/IRAC* were used to maximize the planet emission, which translates to a higher flux dimming. To estimate the eclipse depth we consider both the planet and the star emit as blackbodies, that in the mid-infrared can be approximated by Rayleigh-Jeans taking the form (e.g., [Winn 2010](#); [Encrenaz 2014](#)):

$$\delta_{\text{occ}} = 0.01 \left(\frac{R_p/R_J}{R_{\star}/R_{\odot}} \right)^2 \frac{T_{\text{eq}}}{T_{\star}}, \quad (4)$$

where R_p and R_{\star} are the planet and stellar radius in Jovian and solar units respectively, and T_{eq}/T_{\star} is the planet equilibrium and stellar temperature ratio. With the same assumption, we can also estimate T_{eq} as:

$$T_{\text{eq}} = 279 (1 - a)^{0.25} \left(\frac{T_{\star}/K}{5770} \right) \left(\frac{R_{\text{star}}/R_{\odot}}{D/\text{AU}} \right)^{0.5}, \quad (5)$$

where a is the geometric albedo and D is the planet-star distance in AU. At shorter wavelengths, the reflected emission from the star might be detectable and it also depends on a , D , and R_p . Nonetheless, the occultation depth is maximum at the mid-infrared where this component can be ignored. In Fig. 5, we show

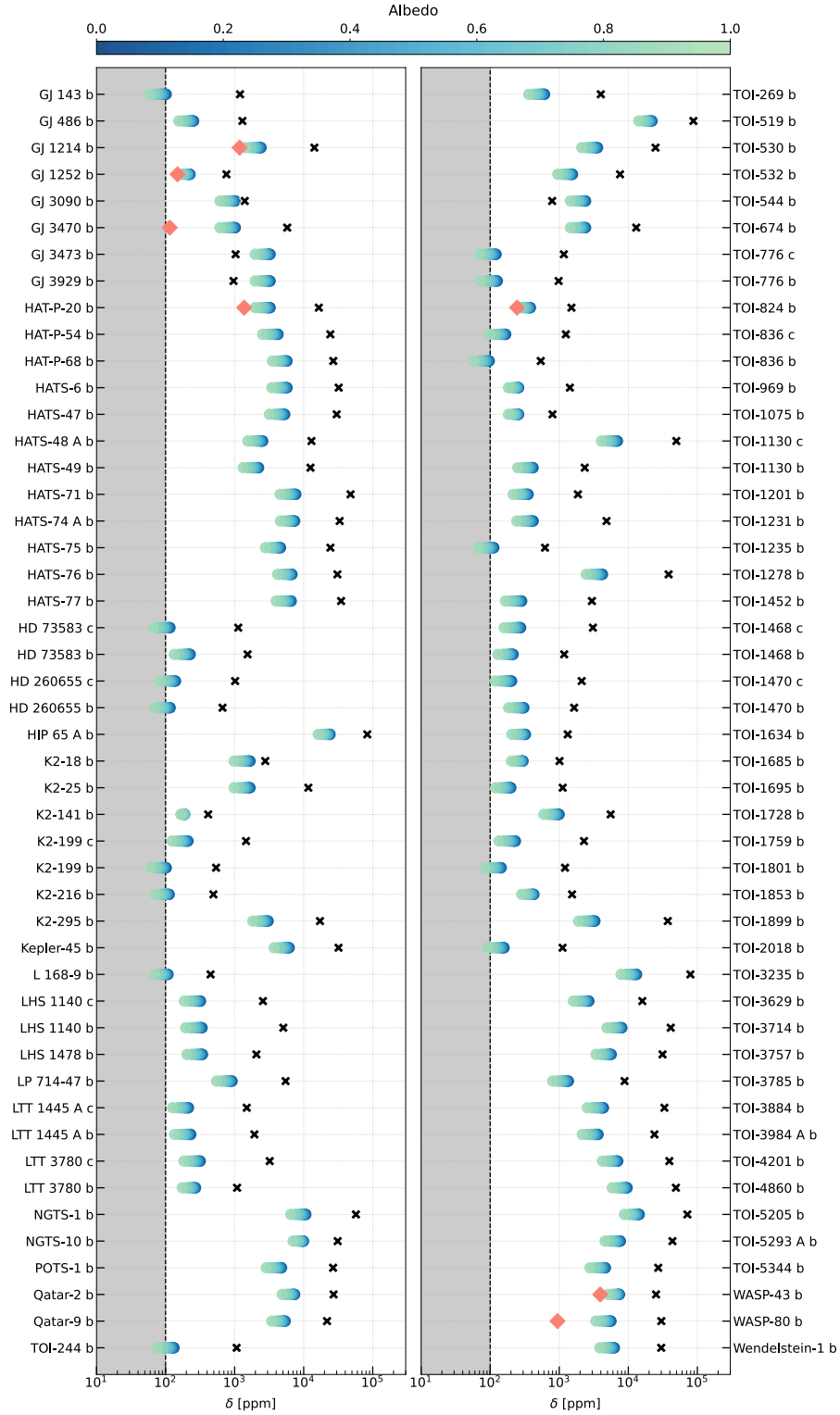


Fig. 5. Depths of the transit (black cross), predicted occultation (color-coded as function of the albedo), and true occultation if measured (salmon diamond) per planet. Dashed line is at 100 ppm, considering the grey area as the undetectable regime by current instrumentation.

the measured transit depths and the estimated occultation depths as a function of the albedo for all the confirmed planets in the sample. For the few targets with this quantity measured, it is also represented here. We have found that they are compatible with the theoretical approximation (except for GJ 3470 b and WASP-80 b), but all of them are overestimated. This is probably because empirically the wavelength used is around $4.5 \mu\text{m}$ but the

thermal emission would be increased at higher wavelengths (e.g., using JWST/MIRI, which covers up to $28 \mu\text{m}$).

Since this study is focused on the low-mass stellar domain, our sample enhances the occultation depth (i.e., $\delta_{\text{occ}} \propto R_{\star}^{-2}$). For this reason, most of the eclipses are expected to be detectable with current instrumentation ($\delta_{\text{occ}} > 100 \text{ ppm}$). We particularly encourage monitoring the secondary eclipse of the weak

candidates resulted from this work, since it would translate in a reduction of the α uncertainty.

6. Conclusions

We have carried out an extensive search for exotrojans around low-mass stars with spectral types later than K4 V. We analyzed publicly available RV time series aiming at identifying mass imbalances within the orbital paths of their confirmed planets. We found a strong candidate for a trojan of $2.6 \pm 0.7 M_{\oplus}$ in the L₅ point of the hot Neptune GJ 3470 b. Additionally, for other two targets which show a weak evidence for the presence of co-orbitals, we also spot a dimming in the predicted Lagrangian point (L₅ for TOI-776 b, and L₄ for TOI-836 b) in their TESS light curves.

The results of the analysis show that the current data permit constraints to be placed on the presence of co-orbitals accompanying planets more massive than Saturn. Interestingly, less massive planets ($<3 M_{\oplus}$, such as GJ 486, LHS 1140, or TOI-244), which have been confirmed using the most precise instruments and a wealth of measurements, highlight the potential for significantly reducing the upper limits of co-orbital masses when using more demanding observational strategies (e.g., strategies devoted to the improvement in the precision of the planetary masses). This would lead to a more refined constraint on the presence of trojans and, consequently, would enhance our ability to infer their occurrence rate.

The sample was divided into different groups based on the resulting α parameter. There is particular interest in the targets classified as WC and SS to continue the RV observations. Among the WC, those targets with fewer (or less precise) RV measurements are particularly promising for further investigation using this technique. These planets exhibit a high degree of uncertainty in α , yet their 63% confidence interval exclusively considers the possibility of a co-orbital scenario (non-null values). Some of these targets include K2-199, TOI-776, TOI-1452, TOI-3757, TOI-3884, and TOI-3984 A. Additionally, all targets classified as SS are highly desirable for continued observation via RV measurements. Special attention is warranted for GJ 1252 and TOI-824, since it is expected to derivate credible α values, given their well-known eccentricity as their secondary transit is measured.

Conversely, for some other targets within the WC group, it is not worthwhile to continue the RV monitoring as the observational cost outweighs the potential for improvements. These candidates need to be studied in more detail through other techniques, such as photometrically inspecting the Lagrangian regions, combining the photometrical observations with dynamical models (e.g., Lillo-Box et al. 2018b), and even directly imaging with future missions such as LIFE (Quanz et al. 2022). Priority should be given to the search for the occultation of the main planet in order to break the degeneracy of the trojan presence with the orbital architecture. Based on the estimation of the occultation depth (Sect. 5.3), the most promising targets (with depths above 10^3 ppm) among the WC to measure the eclipse in infrared light are: GJ 3473 b, K2-18 b, LP 714-47 b, Qatar 2 b, TOI-544 b, TOI-3757 b, TOI-3884 b, and TOI-3984 b.

It is important to note that a null detection in the context of our methodology does not definitively rule out the presence of co-orbital companions, yet it does significantly limit it. Adhering to the tadpole configurations assumption (Sect. 5.1), their masses are already tightly constrained, and further narrowing these limits is not expected. Conversely, it is plausible that co-orbitals could escape our detection approach. For instance, horseshoe

configurations could have α values oscillating to zero at each instance that could result in a false negative provided the libration timescale is shorter than the RV time span. Such scenarios may be detectable through alternative detection methods meriting their exploration in future studies (e.g., RV modulations due to the trojan libration, e.g., Leleu et al. 2015).

This work serves to advocate for the RV monitoring of the stars devoted to the search for co-orbitals. It also provides guidelines that can aid in this objective, and a list of the most relevant targets. As demonstrated in previous works of this series (Lillo-Box et al. 2018a,b), increasing the number of measurements and their precision is crucial. In the present work, WASP-43 b and WASP-80 b suggest that not only an appropriate (i.e., homogeneous) coverage of the orbital phase is needed, but increasing the monitoring on phases close to the transit could benefit the determination of the spectroscopic mid-transit time, which directly translates into a lower uncertainty of the α parameter.

Acknowledgements. We thank to the anonymous referee for their effort reviewing this work. We also thank to all the authors who have helped us to access their data or who have provided relevant information on the targets: J.M. Almenara, C. Cadieux, D. Dragomir, X. Dumusque, E. González-Álvarez, R. Luque, and M. Mallorquín. This research has made use of the NASA Exoplanet Archive, which is operated by the California Institute of Technology, under contract with the National Aeronautics and Space Administration under the Exoplanet Exploration Program. This Project has been funded by grant No.PID2019-107061GB-C61 by the Spanish Ministry of Science and Innovation/State Agency of Research MCIN/AEI/10.13039/501100011033. O.B.-R. is supported by INTA grant PRE-MDM-07. J.L.-B. was partly funded by grants LCF/BQ/PI20/11760023 (La Caixa), Ramón y Cajal fellowship with code RYC2021-031640-I, and CNS2023-144309. P. F. acknowledges the financial support of the SNSF, the work has been carried out within the framework of the National Centre of Competence in Research PlanetS supported by the Swiss National Science Foundation under grant 51NF40_205606. AL acknowledges support from the Swiss NCCR PlanetS and the Swiss National Science Foundation. This work has been carried out within the framework of the NCCR PlanetS supported by the Swiss National Science Foundation under grants 51NF40182901 and 51NF40205606. AL acknowledges support of the Swiss National Science Foundation under grant number TMSGI2_211697. Co-funded by the European Union (ERC, FIERCE, 101052347). Views and opinions expressed are however those of the author(s) only and do not necessarily reflect those of the European Union or the European Research Council. Neither the European Union nor the granting authority can be held responsible for them. This work was supported by FCT – Fundação para a Ciência e a Tecnologia through national funds and by FEDER through COMPETE2020 – Programa Operacional Competitividade e Internacionalização by these grants: UIDB/04434/2020; UIDP/04434/2020. E.H.-C. acknowledges support from grant PRE2020-094770 under project PID2019-109522GB-C51 funded by the Spanish Ministry of Science and Innovation/State Agency of Research, MCIN/AEI/10.13039/501100011033, and by ‘ERDF, A way of making Europe’.

References

- Akana Murphy, J. M., Kosiarek, M. R., Batalha, N. M., et al. 2021, *AJ*, **162**, 294
- Akeson, R. L., Chen, X., Ciardi, D., et al. 2013, *PASP*, **125**, 989
- Almenara, J. M., Bonfils, X., Forveille, T., et al. 2022a, *A&A*, **667**, L11
- Almenara, J. M., Bonfils, X., Otegi, J. F., et al. 2022b, *A&A*, **665**, A91
- Alsubai, K., Tsvetanov, Z. I., Pyrzas, S., et al. 2019, *AJ*, **157**, 224
- Ambikasaran, S., Foreman-Mackey, D., Greengard, L., Hogg, D. W., & O’Neil, M. 2015, *IEEE Trans. Pattern Anal. Mach. Intell.*, **38**, 252
- Artigau, É., Hébrard, G., Cadieux, C., et al. 2021, *AJ*, **162**, 144
- Artigau, É., Cadieux, C., Cook, N. J., et al. 2022, *AJ*, **164**, 84
- Astudillo-Defru, N., Cloutier, R., Wang, S. X., et al. 2020, *A&A*, **636**, A58
- Awiphan, S., Kerins, E., Pichadee, S., et al. 2016, *MNRAS*, **463**, 2574
- Bakos, G. Á., Hartman, J., Torres, G., et al. 2011, *ApJ*, **742**, 116
- Bakos, G. Á., Hartman, J. D., Bhatti, W., et al. 2015, *AJ*, **149**, 149
- Bakos, G. Á., Bayliss, D., Bento, J., et al. 2020, *AJ*, **159**, 267
- Balsalobre-Ruza, O., de Gregorio-Monsalvo, I., Lillo-Box, J., et al. 2023, *A&A*, **675**, A172
- Barragán, O., Gandolfi, D., Dai, F., et al. 2018, *A&A*, **612**, A95
- Barragán, O., Armstrong, D. J., Gandolfi, D., et al. 2022, *MNRAS*, **514**, 1606
- Bayliss, D., Gillen, E., Eig Müller, P., et al. 2018, *MNRAS*, **475**, 4467
- Beard, C., Robertson, P., Kanodia, S., et al. 2022a, *AJ*, **163**, 286
- Beard, C., Robertson, P., Kanodia, S., et al. 2022b, *ApJ*, **936**, 55

- Beaugé, C., Sándor, Z., Érdi, B., & Süli, Á. 2007, *A&A*, 463, 359
- Benneke, B., Knutson, H. A., Lotheringer, J., et al. 2019, *Nat. Astron.*, 3, 813
- Bleick, J., Harrington, J., Madhusudhan, N., et al. 2014, *ApJ*, 781, 116
- Bluhm, P., Luque, R., Espinoza, N., et al. 2020, *A&A*, 639, A132
- Bluhm, P., Pallé, E., Molaverdikhani, K., et al. 2021, *A&A*, 650, A78
- Bonfils, X., Almenara, J. M., Cloutier, R., et al. 2018, *A&A*, 618, A142
- Bonomo, A. S., Desidera, S., Benatti, S., et al. 2017, *A&A*, 602, A107
- Bonomo, A. S., Dumusque, X., Massa, A., et al. 2023, *A&A*, 677, A33
- Borucki, W. J., Koch, D., Basri, G., et al. 2010, *Science*, 327, 977
- Burt, J. A., Nielsen, L. D., Quinn, S. N., et al. 2020, *AJ*, 160, 153
- Burt, J. A., Dragomir, D., Mollière, P., et al. 2021, *AJ*, 162, 87
- Caballero, J. A., González-Álvarez, E., Brady, M., et al. 2022, *A&A*, 665, A120
- Cadioux, C., Doyon, R., Plotnykov, M., et al. 2022, *AJ*, 164, 96
- Cadioux, C., Plotnykov, M., Doyon, R., et al. 2024, *ApJ*, 960, L3
- Cañas, C. I., Stefansson, G., Kanodia, S., et al. 2020, *AJ*, 160, 147
- Cañas, C. I., Kanodia, S., Bender, C. F., et al. 2022, *AJ*, 164, 50
- Cañas, C. I., Kanodia, S., Libby-Roberts, J., et al. 2023, *AJ*, 166, 30
- Castro-González, A., Demangeon, O. D. S., Lillo-Box, J., et al. 2023, *A&A*, 675, A52
- Chaturvedi, P., Bluhm, P., Nagel, E., et al. 2022, *A&A*, 666, A155
- Chen, J., & Kipping, D. 2017, *ApJ*, 834, 17
- Cherubim, C., Cloutier, R., Charbonneau, D., et al. 2023, *AJ*, 165, 167
- Cifuentes, C., Caballero, J. A., Cortés-Contreras, M., et al. 2020, *A&A*, 642, A115
- Cloutier, R., Eastman, J. D., Rodriguez, J. E., et al. 2020a, *AJ*, 160, 3
- Cloutier, R., Rodriguez, J. E., Irwin, J., et al. 2020b, *AJ*, 160, 22
- Cloutier, R., Charbonneau, D., Deming, D., Bonfils, X., & Astudillo-Defru, N. 2021a, *AJ*, 162, 174
- Cloutier, R., Charbonneau, D., Stassun, K. G., et al. 2021b, *AJ*, 162, 79
- Cloutier, R., Greklek-McKeon, M., Wurmser, S., et al. 2024, *MNRAS*, 527, 5464
- Cointepas, M., Almenara, J. M., Bonfils, X., et al. 2021, *A&A*, 650, A145
- Coleman, G. A. L., Leleu, A., Alibert, Y., & Benz, W. 2019, *A&A*, 631, A7
- Correia, A. C. M., Bourrier, V., & Delisle, J. B. 2020, *A&A*, 635, A37
- Couturier, J., Robutel, P., & Correia, A. C. M. 2021, *Celest. Mech. Dyn. Astron.*, 133, 37
- Crossfield, I. J. M., Malik, M., Hill, M. L., et al. 2022, *ApJ*, 937, L17
- Dai, F., Schlaufman, K. C., Reggiani, H., et al. 2023, *AJ*, 166, 49
- Demangeon, O. D. S., Zapatero Osorio, M. R., Alibert, Y., et al. 2021, *A&A*, 653, A41
- Deming, D., Knutson, H., Kammer, J., et al. 2015, *ApJ*, 805, 132
- Díaz, R. F., Ségransan, D., Udry, S., et al. 2016, *A&A*, 585, A134
- Dobrovolskis, A. R., & Lissauer, J. J. 2022, *Icarus*, 385, 115087
- Dragomir, D., Teske, J., Günther, M. N., et al. 2019, *ApJ*, 875, L7
- Dreizler, S., Crossfield, I. J. M., Kossakowski, D., et al. 2020, *A&A*, 644, A127
- Encrenaz, T. 2014, *Philos. Trans. R. Soc. Lond. Ser. A*, 372, 20130083
- Espinoza, N., Pallé, E., Kemmer, J., et al. 2022, *AJ*, 163, 133
- Esposito, M., Covino, E., Desidera, S., et al. 2017, *A&A*, 601, A53
- Essack, Z., Shporer, A., Burt, J. A., et al. 2023, *AJ*, 165, 47
- Faria, J. P., Haywood, R. D., Brewer, B. J., et al. 2016, *A&A*, 588, A31
- Ford, E. B., & Gaudi, B. S. 2006, *ApJ*, 652, L137
- Foreman-Mackey, D., Conley, A., Meierjürgen Farr, W., et al. 2013, emcee: The MCMC Hammer Astrophysics Source Code Library [[record ascl:1303.002](#)]
- Fridlund, M., Georgieva, I. Y., Bonfanti, A., et al. 2024, *A&A*, 684, A12
- Fulton, B. J., Petigura, E. A., Blunt, S., & Sinukoff, E. 2018, *PASP*, 130, 044504
- Gan, T., Lin, Z., Wang, S. X., et al. 2022, *MNRAS*, 511, 83
- Gan, T., Shporer, A., Livingston, J. H., et al. 2020, *AJ*, 159, 160
- García-Melendo, E., & López-Morales, M. 2011, *MNRAS*, 417, L16
- Giocalone, S., Dressing, C. D., Hedges, C., et al. 2022, *AJ*, 163, 99
- Giuppone, C. A., Benítez-Llambay, P., & Beaugé, C. 2012, *MNRAS*, 421, 356
- González-Álvarez, E., Zapatero Osorio, M. R., Caballero, J. A., et al. 2023, *A&A*, 675, A177
- Goździewski, K., & Konacki, M. 2006, *ApJ*, 647, 573
- Haghighipour, N., Capen, S., & Hinse, T. C. 2013, *Celest. Mech. Dyn. Astron.*, 117, 75
- Hartman, J. D., Bayliss, D., Brahm, R., et al. 2015, *AJ*, 149, 166
- Hartman, J. D., Jordán, A., Bayliss, D., et al. 2020, *AJ*, 159, 173
- Hartman, J. D., Bakos, G. Á., Csubry, Z., et al. 2023, *AJ*, 166, 163
- Hawthorn, F., Bayliss, D., Wilson, T. G., et al. 2023, *MNRAS*, 520, 3649
- Hipke, M., & Angerhausen, D. 2015, *ApJ*, 811, 1
- Hipke, M., David, T. J., Mulders, G. D., & Heller, R. 2019, *AJ*, 158, 143
- Hobson, M. J., Jordán, A., Bryant, E. M., et al. 2023, *ApJ*, 946, L4
- Howell, S. B., Sobeck, C., Haas, M., et al. 2014, *PASP*, 126, 398
- Hoyer, S., Pallé, E., Dragomir, D., & Murgas, F. 2016, *AJ*, 151, 137
- Isella, A., Huang, J., Andrews, S. M., et al. 2018, *ApJ*, 869, L49
- Jackson, B., Greenberg, R., & Barnes, R. 2008, *ApJ*, 678, 1396
- Jeffers, S. V., Schöfer, P., Lamert, A., et al. 2018, *A&A*, 614, A76
- Jenkins, J. M., Twicken, J. D., McCauliff, S., et al. 2016, *SPIE Conf. Ser.*, 9913, 99133E
- Johnson, J. A., Gazak, J. Z., Apps, K., et al. 2012, *AJ*, 143, 111
- Jordán, A., Hartman, J. D., Bayliss, D., et al. 2022, *AJ*, 163, 125
- Kagetani, T., Narita, N., Kimura, T., et al. 2023, *PASJ*, 75, 713
- Kanodia, S., Cañas, C. I., Stefansson, G., et al. 2020, *ApJ*, 899, 29
- Kanodia, S., Stefansson, G., Cañas, C. I., et al. 2021, *AJ*, 162, 135
- Kanodia, S., Libby-Roberts, J., Cañas, C. I., et al. 2022, *AJ*, 164, 81
- Kanodia, S., Mahadevan, S., Libby-Roberts, J., et al. 2023, *AJ*, 165, 120
- Kemmer, J., Stock, S., Kossakowski, D., et al. 2020, *A&A*, 642, A236
- Kemmer, J., Dreizler, S., Kossakowski, D., et al. 2022, *A&A*, 659, A17
- Kepton, E. M. R., Zhang, M., Bean, J. L., et al. 2023, *Nature*, 620, 67
- Kiefer, F., Hébrard, G., Martioli, E., et al. 2023, *A&A*, 670, A136
- Knutson, H. A., Fulton, B. J., Montet, B. T., et al. 2014, *ApJ*, 785, 126
- Koppenhoefer, J., Saglia, R. P., Fossati, L., et al. 2013, *MNRAS*, 435, 3133
- Korth, J., Gandolfi, D., Šubjak, J., et al. 2023, *A&A*, 675, A115
- Kosiarek, M. R., Crossfield, I. J. M., Hardegree-Ullman, K. K., et al. 2019, *AJ*, 157, 97
- Kossakowski, D., Kemmer, J., Bluhm, P., et al. 2021, *A&A*, 656, A124
- Kunimoto, M., & Matthews, J. M. 2020, *AJ*, 159, 248
- Laughlin, G., & Chambers, J. E. 2002, *AJ*, 124, 592
- Leleu, A., Robutel, P., & Correia, A. C. M. 2015, *A&A*, 581, A128
- Leleu, A., Robutel, P., Correia, A. C. M., & Lillo-Box, J. 2017, *A&A*, 599, L7
- Leleu, A., Coleman, G. A. L., & Ataiee, S. 2019, *A&A*, 631, A6
- Leleu, A., Alibert, Y., Hara, N. C., et al. 2021a, *A&A*, 649, A26
- Leleu, A., Chatel, G., Udry, S., et al. 2021b, *A&A*, 655, A66
- Libby-Roberts, J. E., Schutte, M., Hebb, L., et al. 2023, *AJ*, 165, 249
- Lightkurve Collaboration (Cardoso, J. V. d. M., et al.) 2018, Lightkurve: Kepler and TESS time series analysis in Python, Astrophysics Source Code Library [[record ascl:1812.013](#)]
- Lillo-Box, J., Barrado, D., Moya, A., et al. 2014, *A&A*, 562, A109
- Lillo-Box, J., Barrado, D., Figueira, P., et al. 2018a, *A&A*, 609, A96 (Paper I)
- Lillo-Box, J., Leleu, A., Parviainen, H., et al. 2018b, *A&A*, 618, A42 (Paper II)
- Lillo-Box, J., Gandolfi, D., Armstrong, D. J., et al. 2023, *A&A*, 669, A109
- Lindor, B. M., Hartman, J. D., Bakos, G. Á., et al. 2021, *AJ*, 161, 64
- Long, F., Andrews, S. M., Zhang, S., et al. 2022, *ApJ*, 937, L1
- Luque, R., & Pallé, E. 2022, *Science*, 377, 1211
- Luque, R., Serrano, L. M., Molaverdikhani, K., et al. 2021, *A&A*, 645, A41
- Luque, R., Fulton, B. J., Kunimoto, M., et al. 2022, *A&A*, 664, A199
- Malavolta, L., Mayo, A. W., Louden, T., et al. 2018, *AJ*, 155, 107
- Mallorquín, M., Goffo, E., Pallé, E., et al. 2023, *A&A*, 680, A76
- Mancini, L., Southworth, J., Ciceri, S., et al. 2014, *MNRAS*, 443, 2391
- McCormac, J., Gillen, E., Jackman, J. A. G., et al. 2020, *MNRAS*, 493, 126
- Ment, K., Dittmann, J. A., Astudillo-Defru, N., et al. 2019, *AJ*, 157, 32
- Murgas, F., Astudillo-Defru, N., Bonfils, X., et al. 2021, *A&A*, 653, A60
- Namouni, F., & Morais, H. 2018, *Comput. Appl. Math.*, 37, 65
- Nielsen, L. D., Brahm, R., Bouchy, F., et al. 2020, *A&A*, 639, A76
- Nowak, G., Luque, R., Parviainen, H., et al. 2020, *A&A*, 642, A173
- Obermeier, C., Steuer, J., Kellermann, H., et al. 2020, *A&A*, 639, A130
- Oddo, D., Dragomir, D., Brandeker, A., et al. 2023, *AJ*, 165, 134
- Osborne, H. L. M., Van Eylen, V., Goffo, E., et al. 2024, *MNRAS*, 527, 11138
- Paredes, L. A., Henry, T. J., Quinn, S. N., et al. 2021, *AJ*, 162, 176
- Persson, C. M., Fridlund, M., Barragán, O., et al. 2018, *A&A*, 618, A33
- Pierens, A., & Raymond, S. N. 2014, *MNRAS*, 442, 2296
- Powers, L. C., Libby-Roberts, J., Lin, A. S. J., et al. 2023, *AJ*, 166, 44
- Quanz, S. P., Ottiger, M., Fontanet, E., et al. 2022, *A&A*, 664, A21
- Radica, M., Artigau, É., Lafrenière, D., et al. 2022, *MNRAS*, 517, 5050
- Ricker, G. R., Winn, J. N., Vanderspek, R., et al. 2014, *SPIE Conf. Ser.*, 9143, 20
- Roy, P.-A., Benneke, B., Piaulet, C., et al. 2022, *ApJ*, 941, 89
- Serrano, L. M., Gandolfi, D., Mustill, A. J., et al. 2022, *Nat. Astron.*, 6, 736
- Shporer, A., Collins, K. A., Astudillo-Defru, N., et al. 2020, *ApJ*, 890, L7
- Smith, A. M. S., Csizmadia, S., Gandolfi, D., et al. 2019, *Acta Astron.*, 69, 135
- Soto, M. G., Anglada-Escudé, G., Dreizler, S., et al. 2021, *A&A*, 649, A144
- Stefansson, G., Mahadevan, S., Maney, M., et al. 2020, *AJ*, 160, 192
- Stefansson, G., Mahadevan, S., Petrovich, C., et al. 2022, *ApJ*, 931, L15
- Sun, L., Gu, S., Wang, X., et al. 2017, *AJ*, 153, 28
- Teske, J., Wang, S. X., Wolfgang, A., et al. 2021, *ApJS*, 256, 33
- Thao, P. C., Mann, A. W., Johnson, M. C., et al. 2020, *AJ*, 159, 32
- Triaud, A. H. M. J., Anderson, D. R., Collier Cameron, A., et al. 2013, *A&A*, 551, A80
- Triaud, A. H. M. J., Gillon, M., Ehrenreich, D., et al. 2015, *MNRAS*, 450, 2279
- Triaud, A. H. M. J., Standing, M. R., Heidari, N., et al. 2022, *MNRAS*, 511, 3561
- Triaud, A. H. M. J., Dransfield, G., Kagitani, T., et al. 2023, *MNRAS*, 525, L98
- Trifonov, T., Caballero, J. A., Morales, J. C., et al. 2021, *Science*, 371, 1038
- Winn, J. N. 2010, in *Exoplanets*, ed. S. Seager (Tucson : Univ. Arizona Press), 55
- Winters, J. G., Cloutier, R., Medina, A. A., et al. 2022, *AJ*, 163, 168

Appendix A: Radial velocity analysis per system

In this section, we give the details of the RV analysis for the individual targets. Full version of this appendix is available in Zenodo⁴.

A.1. Strong candidate

GJ 3470

Located in the hot-Neptune desert, GJ 3470 b has been object of many studies trying to bring light to the rare population to which it belongs. As a result, we account with multiple high-precision RV measurements. The RV analysis requires a linear trend probably caused by an undetected stellar companion, for which we inferred a slope of $(-0.0022 \pm 0.0011) \text{ m s}^{-1} \text{ d}^{-1}$. The secondary eclipse of this planet has been observed, allowing us to set normal priors on the c and d parameters that were derived in this work using the eclipse published in Benneke et al. (2019), and obtaining compatible results with those from Kosiarek et al. (2019) (see Table B.3). Even there is no clear correlation between the RV measurements and the activity indicators, we included a GP informed with the S_{HK} index as it shows a peak in its GLS at $P_{\text{rot}} = 21.5 \pm 0.5 \text{ d}$. The resulting α places this target as a SC with a 3- σ significance.

A.2. Weak candidates

GJ 486

This single-planet target has an α parameter different from 0 in 1- σ in both slightly eccentric ($e < 0.1$) and circular orbit scenarios. We do not include a GP to the analysis since, according with Caballero et al. (2022), none of the periodograms of the activity indicators (e.g., H_{α} , Ca II, or Na I) show any significant peak that could suggest the star is active.

GJ 3473

Our RV analysis for the confirmed planet GJ 3473 b resulted in an α parameter different from 0 within 1- σ for both tested models, the slightly eccentric ($\alpha = -0.30^{+0.23}_{-0.24}$) and the circular orbit ($\alpha = -0.28^{+0.21}_{-0.22}$). Based on the H_{α} emission line, this target is considered inactive (Jeffers et al. 2018).

HD 260655

Both planets in this system transit the star with short periods, lying in a close 2:1 MMR ($P_b = 2.8 \text{ d}$, and $P_c = 5.7 \text{ d}$). However, these rocky worlds do not show significant TTVs according with Luque et al. (2022). Based on the values obtained for the H_{α} emission and R'_{HK} , this star is thought to be inactive with a rotation period of around $\sim 30 \text{ d}$. Our analysis found that, contrary to the inner planet, the outer one has an α parameter different from zero within 1- σ ($\alpha = -0.32^{+0.22}_{-0.25}$) indicating that the mass of its potential co-orbital companion could be higher than the one for the inner planet. This result is hold when considering circular orbits. As warned in Leleu et al. (2017) (and discussed in Sect. 4), planets in 2:1 MMR are susceptible to mimic co-orbitals in the α -test method. Nonetheless, as no TTVs are detected and the RV time span is huge (24 years) in comparison with the orbital periods, a false positive caused by the planetary configuration is not expected. Detailed searches to constrain their presence is needed, such as photometrically inspect the Lagrangian regions in the search for dimmings (see Sect. 5.2).

K2-18

With an orbital period of 32.9 d, K2-18 b is a Super-Earth in the habitable zone (HZ) of an M-dwarf. We use the RVs extracted with the recent line-by-line (LBL) method (Artigau et al. 2022) published in Radica et al. (2022). They identified 14 outliers in CARMENES and three in the HARPS datasets, resulting in a total time series of 147 measurements after discarding those data points. This system has been claimed to host an additional not-transiting planet in a 9.2 d orbit confidently detected with the LBL RVs after rejecting a particular night (December 25, 2016). We include a GP informed with the dLW, indicator showing a peak in the GLS at the estimated stellar rotational period ($\sim 39 \text{ d}$). The analysis suggests the presence of a co-orbital for K2-18 b with an $\alpha = 0.48^{+0.29}_{-0.28}$.

K2-141

K2-141 b is an ultra-short period planet orbiting at 0.28 d. There is an additional validated transiting planet with a period of 7.7 d that is not detected with the RV dataset. Therefore, we carried out the analysis only considering planet b. The RV dataset shows a considerably big scatter. Besides, all the GLS of the activity indicators present a peak at $P_{\text{rot}} = 14 \text{ d}$, so we add a GP by using the FWHM as proxy. Our analysis was compatible with a configuration with an low-mass co-orbital within L_4 as $\alpha = 0.07 \pm 0.07$.

⁴ <https://zenodo.org/records/12636521>

Appendix B: Additional tables

Table B.1. Archival radial velocities and parameters adopted in this work.

System	Planet	Nrvs	$N_{ms}^{(a)}$	Timespan [d]	Transits	P [d]	$T_0 - 2\,450\,000$ [d]	Ref. ^(b) RV / param.
GJ 143	b	283	4	5942.8	Yes	$35.61253^{+0.00060}_{-0.00062}$	$8385.92502^{+0.00054}_{-0.00055}$	Dra19
GJ 486	b	243	7	1967.1	Yes	$1.467119^{+0.00051}_{-0.00051}$	8931.15935 ± 0.00042	Cab22 / Trn21
GJ 1214	b	163	2	3734.8	Yes	$1.58040433 \pm 0.00000013$	$5701.413328^{+0.000066}_{-0.000059}$	Clo21a
GJ 1252	b	20	1	10.9	Yes	$0.51824160 \pm 0.00000069$	8668.09748 ± 0.00032	Shp20 / Luq22b
GJ 3090	b	55	1	326.0	Yes	$2.853136^{+0.00064}_{-0.00064}$	8370.41849 ± 0.00034	Alm22a
GJ 3470	b	193	5	4709.1	Yes	$3.3366496^{+0.000033}_{-0.000033}$	5983.70421 ± 0.00010	Lil18, Ste22 / Awi16
GJ 3473	b	148	3	358.2	Yes	$1.1980035^{+0.000018}_{-0.000019}$	$8492.20408^{+0.00043}_{-0.00042}$	Kem20
	c				No	15.509 ± 0.033	8575.6 ± 2.2	
GJ 3929	b	97	2	528.6	Yes	2.616235 ± 0.000005	8956.39620 ± 0.00050	Bea22, Kem22 / Bea22
	c				No	15.040 ± 0.030	9070.9 ± 2.0	
HAT-P-20	b	57	4	2857.8	Yes	2.8753172 ± 0.0000003	$5917.64480461 \pm 0.00000010$	Bak11, Knu14, Esp17, Lil18 / Sun17
HAT-P-54	b	17	2	410.0	Yes	3.799847 ± 0.000014	6299.3037 ± 0.00024	Bak15
HAT-P-68	b	13	3	1100.0	Yes	$2.29840551 \pm 0.00000052$	6614.20355 ± 0.00014	Lin21
HATS-6	b	15	3	259.2	Yes	3.3252725 ± 0.0000021	6643.74058 ± 0.000084	Har15
HATS-47	b	12	1	151.7	Yes	3.9228038 ± 0.0000022	7365.35804 ± 0.00029	Har20
HATS-48 A	b	11	1	125.8	Yes	3.1316666 ± 0.0000037	7100.55022 ± 0.00045	Har20
HATS-49	b	8	1	536.3	Yes	4.1480467 ± 0.0000037	7105.1648 ± 0.00054	Har20
HATS-71	b	7	1	744.0	Yes	3.7955202 ± 0.0000010	7858.80134 ± 0.00023	Bak20
HATS-74 A	b	5	1	5.0	Yes	1.73185606 ± 0.0000055	8392.02654 ± 0.00024	Jor22
HATS-75	b	5	1	6.1	Yes	2.7886556 ± 0.0000011	8611.05487 ± 0.00027	Jor22
HATS-76	b	3	1	6.1	Yes	1.9416423 ± 0.0000014	8424.55556 ± 0.00053	Jor22
HATS-77	b	5	1	25.9	Yes	3.0876262 ± 0.0000016	9136.69378 ± 0.00020	Jor22
HD 73583	b	87	1	334.1	Yes	$6.398042^{+0.000067}_{-0.000062}$	$8517.69013^{+0.00056}_{-0.00059}$	Tes21, Bar22 / Odd23
	c				Yes	$18.87974^{+0.00074}_{-0.00074}$	$9232.1682^{+0.00019}_{-0.00024}$	Tes21, Bar22 / Bar22
HD 260655	b	180	2	8794.5	Yes	2.76953 ± 0.000030	9497.91020 ± 0.00030	Luq22a
	c				Yes	5.70588 ± 0.000070	9490.36460 ± 0.00040	
HIP 65 A	b	90	3	491.9	Yes	0.9809734 ± 0.00000031	8326.102581 ± 0.000050	Nie20, Par21 / Nie20
K2-18	b	146	2	1189.9	Yes	32.9396 ± 0.0004	7264.39140 ± 0.00070	Rad22
	c				No	$9.207^{+0.007}_{-0.006}$	$7267.581^{+0.480}_{-0.460}$	
K2-25	b	31	1	427.8	Yes	$3.484545^{+0.00043}_{-0.00043}$	$7062.57958^{+0.00054}_{-0.00056}$	Ste20 / Tha20
K2-141	b	74	2	1500.9	Yes	0.2803244 ± 0.0000015	7744.07160 ± 0.00022	Bar18, Mal18, Bon23 / Bon23
	c				Yes	7.7485 ± 0.00022	7751.1546 ± 0.001	
K2-199	b	45	1	1071.0	Yes	3.2253993 ± 0.0000024	$7218.7373^{+0.00051}_{-0.00055}$	Aka21
	c				Yes	7.3744897 ± 0.0000037	7222.93034 ± 0.00035	Aka21

Table B.1. Continued.

System	Planet	NRVs	$N_{\text{ins}}^{(b)}$	Timespan [d]	Transits	P [d]	$T_0 - 2\,450\,000$ [d]	Ref. ^(b) RV / param.
K2-216	b	26	4	488.7	Yes	2.1748 ± 0.000050	7394.04170 ± 0.00090	Per18
K2-295	b	6	1	108.7	Yes	4.024867 ± 0.000015	7395.4140500 ± 0.0000010	Smi19
Kepler-45	b	14	1	92.7	Yes	2.455239 ± 0.0000040	5003.822000 ± 0.000036	Joh12
L 168-9	b	123	2	106.0	Yes	1.4015 ± 0.00018	8340.04781 ^{+0.00088} -0.00122	Ast20
LHS 1140	b	254	3	1470.9	Yes	24.737230 ± 0.000020	8399.93000 ± +0.00030	Men19, Cad24 / Cad24
	c				Yes	3.777940 ± 0.000020	8389.29390 ± +0.00020	Men19, Cad24 / Cad24
LHS 1478	b	57	1	261.3	Yes	1.9495378 ^{+0.000040} -0.000041	8786.75425 ± 0.00042	Sof21
LP 714-47	b	81	5	314.5	Yes	4.052037 ± 0.0000040	9196.11490 ^{+0.00031} -0.00030	Dre20
LTT 1445 A	b	135	5	643.4	Yes	5.3587657 ^{+0.000043} -0.000042	8412.70851 ^{+0.00040} -0.00039	Win22 / Odd23
	c				Yes	3.1239032 ^{+0.000036} -0.000035	8412.58159 ^{+0.00057} -0.00057	Win22
LTT 3780	b	119	4	267.1	Yes	0.768448 ^{+0.000055} -0.000053	8543.9115 ± 0.0011	Now20, Clo20a / Luq22b
	c				Yes	12.2519 ^{+0.0028} -0.0030	8546.8484 ± 0.0014	Now20, Clo20a / Luq22b
NGTS-1	b	7	1	10.9	Yes	2.647298 ± 0.000020	7720.659396 ± 0.00062	Bay18
NGTS-10	b	10	1	413.8	Yes	0.7668944 ± 0.0000030	7518.84377 ± 0.00017	McC20
POTS-1	b	13	2	462.9	Yes	3.1606296 ± 0.0000016	4231.65488 ± 0.00044	Kop13
Qatar-2	b	80	4	2365.6	Yes	1.33711647 ± 0.00000026	5624.267096 ± 0.000087	Bon17, Esp17 / Man14
Qatar-9	b	9	1	107.9	Yes	1.540731 ± 0.000038	8227.75643 ± 0.00027	Als19
TOI-244	b	57	1	357.9	Yes	7.397225 ± 0.000026	8357.3627 ± 0.0020	Cas23
TOI-269	b	81	1	275.2	Yes	3.6971104 ± 0.0000037	2458381.84668 ± 0.00033	Co121
TOI-519	b	17	1	265.2	Yes	1.2652328 ± 0.0000050	8491.877117 ± 0.00013	Kag23
TOI-530	b	15	1	9.0	Yes	6.387597 ^{+0.000019} -0.000018	8470.1998 ^{+0.0016} -0.0017	Gan22
TOI-532	b	18	1	134.8	Yes	2.3266508 ± 0.0000030	8470.57678 ^{+0.00066} -0.00066	Kan21
TOI-544	b	122	2	1051.2	Yes	1.5483510 ± 0.0000015	8469.75700 ± 0.00050	Os23 / Gia22
	c				No	50.089 ± 0.24	9212.0 ± 1.9	Os23
TOI-674	b	17	1	54.9	Yes	1.9771430 ± 0.0000030	8641.404552 ± 0.00010	Mur21
TOI-776	b	64	2	545.7	Yes	8.246620 ^{+0.000024} -0.000031	9288.8713 ^{+0.0010} -0.0011	Fri24
	c				Yes	15.665323 ^{+0.000075} -0.000070	9324.53478 ^{+0.00080} -0.00077	Fri24
TOI-824	b	17	2	39.9	Yes	1.392978 ^{+0.000015} -0.000015	8639.60354 ± 0.00035	Bur20
TOI-836	b	52	1	351.1	Yes	3.816730 ± 0.000010	8599.9953 ± 0.0019	Haw23
	c				Yes	8.595450 ± 0.000010	8599.76230 ± 0.00080	
TOI-969	b	73	2	141.7	Yes	1.8237305 ^{+0.000020} -0.000021	9248.37709 ^{+0.00036} -0.00039	Lil23
	c				No	1700.0 ^{+290.0} -280.0	10640.0 ± 260.0	Lil23
TOI-1075	b	54	1	176.7	Yes	0.6047328 ± 0.0000032	8654.25100 ^{+0.00040} -0.00050	Ess23
TOI-1130	b	48	1	62.0	Yes	4.07445 ± 0.000046	8658.7405 ± 0.0013	Kor23
	c				Yes	8.350381 ^{+0.000032} -0.000033	8657.90322 ± 0.00030	Kor23

Table B.1. Continued.

System	Planet	N _{obs}	N _{lim} ^(a)	Timespan [d]	Transits	P [d]	T ₀ - 2 450 000 [d]	Ref. ^(b) RV / param.
TOI-1201	b	33	1	100.8	Yes	2.4919863 ^{+0.0000030} _{-0.0000030}	9169.23222 ^{+0.00052} _{-0.00052}	Kos21
TOI-1231	b	14	1	272.3	Yes	24.245586 ^{+0.00064} _{-0.00064}	8685.11630 ^{+0.00048} _{-0.00048}	Bur21
TOI-1235	b	97	3	128.9	Yes	3.444717 ^{+0.000040} _{-0.000042}	8683.6155 ^{+0.00017} _{-0.00015}	Blu20, Clo20b / Luq22b
TOI-1278	b	10	1	154.7	Yes	14.47567 ± 0.00021	8711.9595 ± 0.0013	Art21
TOI-1452	b	52	1	124.8	Yes	11.06201 ± 0.000020	8691.5321 ± 0.0015	Cad22
TOI-1468	b	81	2	686.4	Yes	1.8805136 ^{+0.0000024} _{-0.0000026}	8765.68079 ^{+0.00007} _{-0.00069}	Cha22
	c				Yes	15.532482 ^{+0.000034} _{-0.000033}	8766.9269 ± 0.0012	Cha22
TOI-1470	b	43	1	228.7	Yes	2.527093 ± 0.000040	8766.47020 ± 0.00060	Gon23
TOI-1634	b	32	1	209.7	Yes	0.989343 ± 0.000015	8791.51473 ± 0.00061	Clo21b / Luq22b
TOI-1685	b	91	2	206.1	Yes	0.6691403 ^{+0.0000023} _{-0.0000023}	8816.22615 ^{+0.00050} _{-0.0006}	Blu21, Luq22b / Luq22b
TOI-1695	b	220	2	417.4	Yes	3.1342791 ^{+0.0000071} _{-0.0000063}	8791.5206 ^{+0.0011} _{-0.0011}	Che23, Kie23 / Che23
TOI-1728	b	30	1	52.0	Yes	3.49151 ^{+0.000062} _{-0.000057}	8843.27427 ± 0.00043	Kan20
TOI-1759	b	57	1	177.7	Yes	18.85019 ± 0.00013	8745.4654 ± 0.0011	Esp22
TOI-1801	b	109	2	585.7	Yes	10.64386 ^{+0.00005} _{-0.00006}	2 458 903.54333 ^{+0.00337} _{-0.00340}	Mal23
TOI-1899	b	15	1	56.9	Yes	29.02 ^{+0.36} _{-0.23}	8711.9578 ± 0.0012	Cañ20
TOI-2018	b	38	1	3725.9	Yes	7.435583 ± 0.000022	8958.258 ± 0.0013	Dia23
TOI-3235	b	7	1	12.1	Yes	2.59261842 ± 0.00000041	9690.00173 ± 0.000045	Hob23
TOI-3629	b	28	2	361.0	Yes	3.936551 ^{+0.0000050} _{-0.0000060}	8784.256 ± 0.0010	Cañ22
TOI-3714	b	26	3	136.0	Yes	2.154849 ± 0.000010	8840.5093 ± 0.00040	Cañ22, Har23 / Cañ22
TOI-3757	b	27	2	130.9	Yes	3.438753 ± 0.0000040	8838.77148 ^{+0.00062} _{-0.00061}	Kan22
TOI-3785	b	39	2	557.7	Yes	4.674737 ± 0.0000038	8861.49553 ± 0.00060	Pow23
TOI-3884	b	19	2	222.5	Yes	4.5445697 ± 0.0000094	9642.86314 ± 0.00012	Alm22b, Lib23 / Alm22b
TOI-3984 A	b	41	2	260.1	Yes	4.353326 ± 0.0000050	9715.022680 ± 0.000095	Cañ23
TOI-4201	b	12	1	122.9	Yes	3.5819134 ± 0.0000017	8470.96190 ± 0.00040	Har23
TOI-4860	b	7	1	26.1	Yes	1.52275959 ± 0.00000035	9832.641439 ± 0.000032	Tri23
TOI-5205	b	7	1	28.9	Yes	1.630757 ± 0.0000010	9443.47179 ± 0.00019	Kan23
TOI-5293 A	b	16	1	60.8	Yes	2.930289 ± 0.0000040	9448.91480 ± 0.00040	Cañ23
TOI-5344	b	13	1	130.9	Yes	3.7926220 ± 0.0000062	9848.99030 ± 0.00019	Har23
WASP-43	b	246	2	2898.3	Yes	0.8134750 ± 0.0000010	5528.86774 ± 0.00014	ESO Archive ^c / Hoy16
WASP-80	b	54	2	776.8	Yes	3.06785234 ^{+0.0000083} _{-0.0000079}	6487.425006 ^{+0.00023} _{-0.00025}	Tri13 / Tri15
Wendelstein-1	b	9	2	1443.9	Yes	2.6634160 ± 0.0000010	5367.738464 ± 0.000014	Obe20

Notes. ^(a)We consider as two different instruments a single instrument with a change in the offset at a given epoch (e.g., caused by an instrumental upgrade). ^(b)Aka21: Akana Murphy et al. (2021); Alm22a: Almenara et al. (2022b); Alm22b: Almenara et al. (2022a); Als19: Alsubai et al. (2019); Art21: Artigau et al. (2019); Ast20: Astudillo-Defru et al. (2020); Awi16: Awiphan et al. (2016); Bak11: Bakos et al. (2011); Bak15: Bakos et al. (2015); Bak20: Bakos et al. (2020); Bay18: Bayliss et al. (2018); Bar18: Barragán et al. (2018); Bar22: Barragán et al. (2022); Bea22: Beard et al. (2022b); Blu20: Bluhm et al. (2020); Blu21: Bluhm et al. (2021); Bon17: Bonomo et al. (2017); Bon23: Bonomo et al. (2023); Bur20: Burt et al. (2020); Bur21: Burt et al. (2021); Cab22: Caballero et al. (2022); Cad22: Cadieux et al. (2022); Cad24: Cadieux et al. (2024); Cas23: Castro-González et al. (2023); Cañ20: Cañas et al. (2020); Cañ22: Cañas et al. (2022); Cañ23: Cañas et al. (2023); Cha22: Chaturvedi et al. (2022); Che23: Cherubim et al. (2023); Clo20a: Cloutier et al. (2020a); Clo20b: Cloutier et al. (2020b); Clo21a: Cloutier et al. (2021a); Clo21b: Cloutier et al. (2021b); Coi21: Coitepas et al. (2021); Dai23: Dai et al. (2023); Dra19: Dragomir et al. (2019); Dre20: Dreizler et al. (2020); Ess23: Essack et al. (2023); Esp17: Esposito et al. (2017); Esp22: Espinoza et al. (2022); Fri24: Fridlund et al. (2024); Gan22: Gan et al. (2022); Gia22: Giacalone et al. (2022); Gon23: González-Álvarez et al. (2023); Har15: Hartman et al. (2015); Har20: Hartman et al. (2020); Har23: Hartman et al. (2023); Haw23: Hawthorn et al. (2023); Hob23: Hobson et al. (2023); Hoy16: Hoyer et al. (2016); Joh12: Johnson et al. (2012); Jor22: Jordán et al. (2022); Kag23: Kagetani et al. (2023); Kan20: Kanodia et al. (2020); Kan21: Kanodia et al. (2021); Kan22: Kanodia et al. (2022); Kan23: Kanodia et al. (2023); Kem20: Kemmer et al. (2020); Kem22: Kemmer et al. (2022); Kie23: Kiefer et al. (2023); Knu14: Knutson et al. (2014); Kop13: Koppenhoefer et al. (2013); Kor23: Korth et al. (2023); Kos21: Kossakowski et al. (2021); Lib23: Libby-Roberts et al. (2023); Lil18: Lillo-Box et al. (2018b); Lil23: Lillo-Box et al. (2023); Lin21: Lindor et al. (2021); Luq22a: Luque et al. (2022); Luq22b: Luque & Pallé (2022); Mal18: Malavolta et al. (2018); Mal23: Mallorquín et al. (2023); Man14: Mancini et al. (2014); McC20: McCormac et al. (2020); Men19: Ment et al. (2019); Mur21: Murgas et al. (2021); Nie20: Nielsen et al. (2020); Now20: Nowak et al. (2020); Obe20: Obermeier et al. (2020); Odd23: Oddo et al. (2023); Osb23: Osborne et al. (2023); Osborn24: Osborn et al. (2024); Par21: Paredes et al. (2021); Per18: Persson et al. (2018); Pow23: Powers et al. (2023); Rad22: Radica et al. (2022); Smi19: Smith et al. (2019); Sof21: Soto et al. (2021); Sph20: Shporer et al. (2020); Ste20: Stefansson et al. (2020); Ste22: Stefansson et al. (2022); Sun17: Sun et al. (2017); Tes21: Teske et al. (2021); Tho20: Thao et al. (2020); Tri13: Triaud et al. (2013); Tri15: Triaud et al. (2015); Tri21: Trifonov et al. (2021); Tri23: Triaud et al. (2023); Win22: Winters et al. (2022). ^(c)http://archive.eso.org/eso_archive_main.html

Table B.2. Radial velocity datasets per system.

System	JD	RV [m/s]	Δ RV[m/s]	Instrument
GJ 1214	2454993.76749	- 8.239	2.275	HARPS pre-upgrade
GJ 1214	2455036.57373	- 18.365	2.503	HARPS pre-upgrade
GJ 1214	2455036.65153	- 13.028	2.385	HARPS pre-upgrade
GJ 1214	2455037.58578	4.096	2.272	HARPS pre-upgrade
GJ 1214	2455037.65309	- 9.916	2.048	...

Notes. Full table is available at the CDS.

Table B.3. Eccentricity constrained by secondary eclipses.

Planet	$e \cos \omega^a$	$e \sin \omega^a$	e	Ref. occ. ^b
GJ 1214 b	-0.00094 ± 0.00018	-0.0005 ± 0.0029	0.0011 ± 0.0014	Kem23
GJ 1252 b	-0.0027 ± 0.0058	-0.012 ± 0.012	0.012 ± 0.012	Cro22
GJ 3470 b	-0.019 ± 0.007	0.001 ± 0.178	0.019 ± 0.014	Ben19
HAT-P-20 b	-0.01352 ± 0.00060	0.0170 ± 0.0034	0.0217 ± 0.0027	Dem15
TOI-824 b	0.0001 ± 0.0083	-0.0003 ± 0.0083	0.0003 ± 0.0042	Roy22
WASP-43 b	-0.049 ± 0.011	-0.03 ± 0.14	0.057 ± 0.076	Ble14
WASP-80 b	-0.023 ± 0.001	-0.007 ± 0.014	0.024 ± 0.004	Tri15

Notes. ^(a)Orbital parameters referred to the planet frame (transit at a true anomaly $\nu = -90^\circ$). ^(b) Ben19: [Benneke et al. \(2019\)](#); Ble14: [Blecic et al. \(2014\)](#); Cro22: [Crossfield et al. \(2022\)](#); Dem15: [Deming et al. \(2015\)](#); Kem23: [Kempton et al. \(2023\)](#); Roy22: [Roy et al. \(2022\)](#); Tri15: [Triaud et al. \(2015\)](#)

Table B.4. Results of the α parameter per model and upper limit to the trojan mass.

Planet	α					Best model	$ \alpha / \sigma_\alpha$	$m_p [M_\oplus]$	Upper limit Trojan mass [M_\oplus]	
	e	c	GPe	GPc	L ₄				L ₅	
Strong Candidates										
GJ 3470 b	-0.17 ± 0.05		-0.16 ± 0.05			GPe	3.2	13.9	0.0	4.1
Weak Candidates										
GJ 486 b	-0.05 ± 0.05	-0.02 ± 0.02				c	1.2	2.8	0.0	0.2
GJ 3473 b	-0.30 ^{+0.23} _{-0.24}	-0.28 ^{+0.21} _{-0.22}				c	1.2	1.9	0.3	1.6
HD 260655 c	-0.32 ^{+0.22} _{-0.25}	-0.34 ^{+0.20} _{-0.23}				c	1.5	3.1	0.2	3.0
K2-18 b	0.38 ^{+0.28} _{-0.26}	0.39 ^{+0.28} _{-0.26}	0.31 ^{+0.30} _{-0.28}	0.48 ^{+0.29} _{-0.28}		GPc	1.7	8.9	9.8	0.9
K2-141 b	-0.13 ^{+0.26} _{-0.25}	-0.13 ^{+0.24} _{-0.23}	-0.04 ^{+0.11} _{-0.09}	0.07 ± 0.07		GPc	1.0	5.1	1.3	0.4
K2-199 c	-0.25 ^{+0.23} _{-0.24}	-0.26 ^{+0.20} _{-0.21}				c	1.2	12.4	2.3	10.3
LHS 1140 b	0.10 ± 0.11	0.14 ^{+0.10} _{-0.11}	-0.06 ^{+0.02} _{-0.06}	-0.11 ^{+0.07} _{-0.02}		GPc	1.5	6.4	0.2	1.2
LHS 1140 c	0.06 ^{+0.16} _{-0.17}	0.01 ± 0.12	0.08 ^{+0.03} _{-0.07}	-0.04 ± 0.02		GPc	1.8	1.8	0.0	0.2
LP 714-47 b	-0.15 ± 0.09	-0.12 ± 0.05				c	2.2	30.8	0.0	8.1
LTT 3780 b	-0.20 ^{+0.16} _{-0.17}	-0.22 ± 0.13				c	1.7	2.6	0.1	1.5
Qatar-2 b	-0.05 ± 0.03	-0.02 ± 0.02				c	1.0	792.6	14.2	50.3
TOI-269 b	0.27 ^{+0.22} _{-0.21}	0.29 ^{+0.20} _{-0.18}				c	1.5	8.8	7.3	0.8
TOI-544 b	0.43 ^{+0.33} _{-0.36}	0.43 ^{+0.32} _{-0.35}	0.57 ^{+0.19} _{-0.24}	0.57 ^{+0.19} _{-0.22}		GPc	2.6	2.9	3.1	0.0
TOI-776 b	-0.62 ^{+0.31} _{-0.25}	-0.62 ^{+0.29} _{-0.24}				c	2.1	4.0	0.1	4.5
TOI-836 b	0.32 ^{+0.40} _{-0.43}	0.33 ^{+0.37} _{-0.39}	0.38 ^{+0.16} _{-0.14}	0.38 ^{+0.16} _{-0.14}		GPc	2.4	4.5	3.7	0.0
TOI-836 c	-0.45 ^{+0.39} _{-0.34}	-0.48 ^{+0.38} _{-0.33}	-0.71 ^{+0.28} _{-0.20}	-0.74 ^{+0.27} _{-0.18}		GPc	2.8	9.6	0.0	11.0
TOI-1130 b	-0.11 ^{+0.17} _{-0.18}	-0.44 ^{+0.12} _{-0.11}				c	3.6	19.3	0.0	15.7
TOI-1130 c	-0.00 ± 0.02	-0.09 ± 0.01				c	9.0	309.6	0.0	38.9
TOI-1235 b	0.23 ^{+0.25} _{-0.23}	0.22 ^{+0.23} _{-0.20}	0.10 ± 0.15	0.12 ^{+0.12} _{-0.11}		GPc	1.0	5.9	2.5	0.7
TOI-1452 b	-0.51 ^{+0.33} _{-0.30}					e	1.5	4.8	1.2	5.4
TOI-1695 b	-0.34 ^{+0.40} _{-0.19}	-0.40 ^{+0.14} _{-0.16}				c	2.5	6.4	0.0	5.4
TOI-3757 b	-0.27 ± 0.17	-0.25 ± 0.13				c	1.9	85.3	0.6	52.6
TOI-3884 b	-0.42 ^{+0.27} _{-0.28}	-0.41 ^{+0.25} _{-0.27}				c	1.5	16.5	2.8	17.5
TOI-3984 A b	0.34 ± 0.28	0.34 ^{+0.27} _{-0.26}				c	1.3	44.5	44.9	11.5
WASP-43 b	-0.007 ± 0.005					e	1.5	565.7	1.7	10.6
Inconclusive										
GJ 143 b	-0.17 ^{+0.08} _{-0.09}		-0.27 ^{+0.44} _{-0.40}			GPe	0.6	22.7	19.1	24.5
GJ 3929 b	-0.13 ^{+0.35} _{-0.38}	-0.14 ^{+0.33} _{-0.36}				c	0.4	1.8	1.2	1.7
HD 73583 b	-0.29 ^{+0.46} _{-0.41}	-0.29 ^{+0.39} _{-0.41}	-0.11 ± 0.41	-0.02 ^{+0.06} _{-0.05}		GPc	0.3	10.2	9.4	10.6
HD 73583 c	0.41 ^{+0.36} _{-0.39}	0.42 ^{+0.35} _{-0.39}	0.25 ^{+0.33} _{-0.28}	-0.02 ^{+0.06} _{-0.05}		GPc	0.7	9.7	10.5	5.1

Table B.4. Continued.

Planet	α			Best model	$ e / \sigma_e$	$m_p [M_\oplus]$	Upper limit Trojan mass [M_\oplus]		
	e	c	GPc				L ₄	L ₅	
HD 260655 b	0.17 ± 0.23	$0.14^{+0.21}_{-0.20}$		c	0.7	2.1	1.5	0.7	
K2-25 b	$-0.22^{+0.50}_{-0.46}$	$-0.22^{+0.50}_{-0.46}$	$-0.18^{+0.61}_{-0.52}$	GPc	0.7	24.5	22.8	27.4	
K2-199 b	0.02 ± 0.32	$0.01^{+0.30}_{-0.29}$		c	0.0	6.9	5.5	5.2	
L 168-9 b	0.08 ± 0.19	-0.05 ± 0.16		c	0.3	4.6	2.1	1.6	
LHS 1478 b	$0.15^{+0.22}_{-0.23}$	0.10 ± 0.20		c	0.5	2.3	1.5	0.9	
TOI-532 b	$0.07^{+0.25}_{-0.27}$	0.02 ± 0.25		c	0.1	61.5	39.6	39.4	
TOI-969 b	$0.21^{+0.31}_{-0.28}$	$0.20^{+0.29}_{-0.2}$	$0.06^{+0.19}_{-0.18}$	GPc	0.2	9.1	4.1	2.7	
TOI-1468 b	0.00 ± 0.21	0.04 ± 0.19	$-0.05^{+0.22}_{-0.10}$	GPc	0.8	3.2	1.2	0.7	
TOI-1468 c	$-0.19^{+0.26}_{-0.27}$	-0.20 ± 0.25	$0.03^{+0.11}_{-0.22}$	GPc	0.0	6.6	1.8	3.0	
TOI-1470 b	$-0.12^{+0.29}_{-0.28}$	$-0.13^{+0.28}_{-0.25}$	-0.20 ± 0.20	GPc	0.9	7.3	1.3	5.2	
TOI-1470 c	$-0.14^{+0.28}_{-0.29}$	$-0.13^{+0.28}_{-0.29}$	$0.30^{+0.43}_{-0.47}$	GPc	0.9	7.2	8.0	4.9	
TOI-1685 b	$0.16^{+0.21}_{-0.20}$	$0.25^{+0.24}_{-0.21}$	0.22 ± 0.17	GPc	0.7	3.8	3.4	1.8	
TOI-1728 b	$-0.23^{+0.25}_{-0.29}$	$-0.22^{+0.23}_{-0.29}$	$-0.23^{+0.24}_{-0.27}$	c	0.8	26.8	7.3	26.3	
TOI-1759 b	$-0.17^{+0.37}_{-0.38}$		$-0.05^{+0.33}_{-0.25}$	GPc	0.9	10.8	3.4	10.2	
TOI-1801 b	-0.10 ± 0.30		$0.24^{+0.21}_{-0.16}$	GPc	0.1	5.7	4.3	4.3	
TOI-2018 b	$0.27^{+0.34}_{-0.31}$	$0.28^{+0.32}_{-0.29}$		GPc	0.6	9.2	9.1	4.4	
TOI-3785 b	$-0.33^{+0.36}_{-0.34}$	-0.33 ± 0.33		c	1.0	15.0	7.4	16.0	
Null Detections									
GJ 1214 b	0.01 ± 0.04			e	0.3	8.2	0.8	0.6	
HAT-P 20 b	0.000 ± 0.002			e	0.0	2302.9	11.9	11.7	
HIP 65 A b ^e	0.01 ± 0.01	0.002 ± 0.004		c	0.5	1021.2	13.8	8.4	
LTT 1445 A b	$-0.02^{+0.12}_{-0.13}$	-0.07 ± 0.08		c	0.8	2.9	0.3	0.8	
LTT 1445 A c	$0.06^{+0.18}_{-0.16}$	$0.10^{+0.14}_{-0.13}$		c	0.7	1.5	0.7	0.3	
LTT 3780 c	$0.04^{+0.13}_{-0.14}$	$0.04^{+0.13}_{-0.14}$		c	0.3	8.6	2.9	2.4	
TOI-244 b	$-0.32^{+0.36}_{-0.35}$	-0.29 ± 0.34	-0.03 ± 0.16	GPc	0.1	2.7	0.7	0.8	
TOI-1075 b	$0.12^{+0.15}_{-0.17}$	0.07 ± 0.13		c	0.5	10.0	3.9	2.5	
TOI-3629 b	$-0.04^{+0.17}_{-0.16}$	-0.01 ± 0.13		c	0.1	82.6	22.6	28.2	
WASP-80 b	-0.03 ± 0.04			e	0.8	171.0	8.7	19.4	
Sparsely Sampled									
GJ 1252 b	$0.32^{+0.38}_{-0.48}$								
HAT-P-54 b	$0.07^{+0.22}_{-0.23}$	0.04 ± 0.07							
HAT-P-68 b	0.12 ± 0.15	$0.07^{+0.11}_{-0.10}$							
HATS-6 b	$0.27^{+0.31}_{-0.29}$	$0.28^{+0.29}_{-0.26}$							

Table B.4. Continued.

Planet	α		Best model	$ e /\sigma_e$	$m_p [M_\oplus]$	Upper limit Trojan mass [M_\oplus]	
	e	c				L ₄	L ₅
HATS-47 b	-0.22 ^{+0.48} -0.42	-0.23 ^{+0.48} -0.41					
HATS-48 A b	-0.48 ^{+0.24} -0.23	-0.46 ^{+0.21} -0.23					
HATS-49 b	-0.35 ^{+0.40} -0.31	-0.38 ^{+0.40} -0.30					
HATS-71 b	0.56 ^{+0.34} -0.69	0.58 ^{+0.32} -0.69					
HATS-74 A b	0.05 ^{+0.12} -0.14	0.01 ± 0.03					
HATS-75 b	-0.01 ^{+0.11} -0.10	-0.01 ± 0.07					
HATS-76 b	0.08 ± 0.07	0.08 ^{+0.05} -0.06					
HATS-77 b	-0.03 ^{+0.12} -0.09	0.06 ^{+0.04} -0.05					
K2-216 b	0.40 ^{+0.30} -0.34	0.40 ^{+0.28} -0.33					
K2-295 b	-0.16 ^{+0.44} -0.34	-0.12 ^{+0.44} -0.37					
Kepler-45 b	-0.25 ^{+0.17} -0.19	-0.29 ^{+0.14} -0.17					
NGTS-1 b	0.05 ^{+0.12} -0.13	0.01 ^{+0.06} -0.05					
NGTS-10 b	0.01 ± 0.04	0.00 ^{+0.01} -0.02					
POTS-1 b	-0.03 ^{+0.68} -0.65	-0.06 ^{+0.68} -0.63					
Qatar-9 b	-0.36 ^{+0.30} -0.28	-0.39 ^{+0.26} -0.23					
TOI-519 b	-0.03 ± 0.14	-0.04 ^{+0.08} -0.07					
TOI-530 b	0.43 ^{+0.23} -0.22	0.52 ^{+0.22} -0.23					
TOI-674 b	0.17 ^{+0.18} -0.19	0.19 ^{+0.13} -0.15					
TOI-776 c	0.16 ^{+0.27} -0.29	0.15 ^{+0.27} -0.29					
TOI-824 b	0.16 ^{+0.12} -0.11						
TOI-1201 b	-0.14 ± 0.32	-0.12 ^{+0.29} -0.30					
TOI-1231 b	-0.23 ± 0.27						
TOI-1278 b	-0.01 ± 0.02						
TOI-1634 b	0.08 ^{+0.27} -0.28	0.01 ± 0.25					
TOI-1899 b	0.23 ^{+0.24} -0.22						
TOI-3235 b	-0.05 ± 0.09	-0.03 ± 0.02					
TOI-3714 b	0.08 ^{+0.08} -0.10	0.02 ^{+0.06} -0.05					
TOI-4201 b	-0.03 ^{+0.07} -0.06	0.09 ^{+0.03} -0.04					
TOI-4860 b	0.27 ^{+0.28} -0.33	0.23 ^{+0.26} -0.30					
TOI-5205 b	-0.16 ^{+0.13} -0.11	-0.07 ± 0.05					
TOI-5293 b	-0.02 ± 0.18	-0.03 ± 0.17					
TOI-5344 b	0.10 ^{+0.13} -0.12	0.14 ^{+0.10} -0.09					
Wendelstein-1 b	-0.05 ^{+0.27} -0.28	-0.04 ^{+0.23} -0.27					

Appendix C: Additional figures

This appendix showing the complete figures is available in Zenodo⁵.

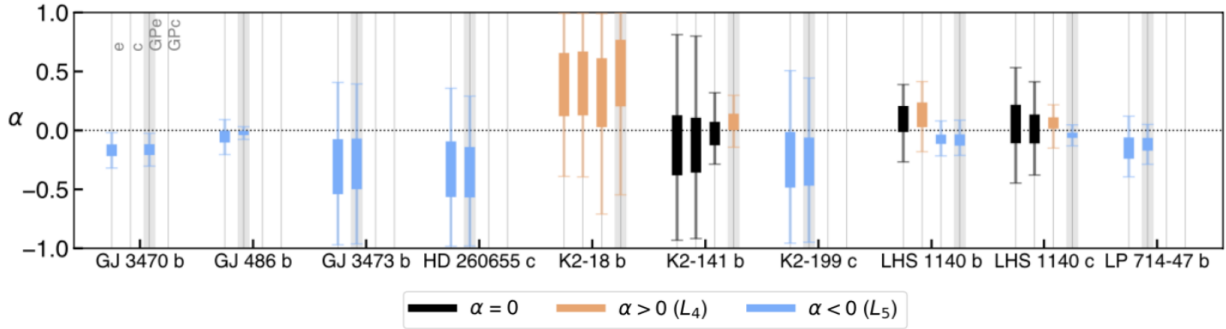


Fig. C.1. Inferred α parameter for the transiting planets grouped as SC, WC, INC, and ND (fragment). **Fig. C.2.** shows this diagram for the SS group.

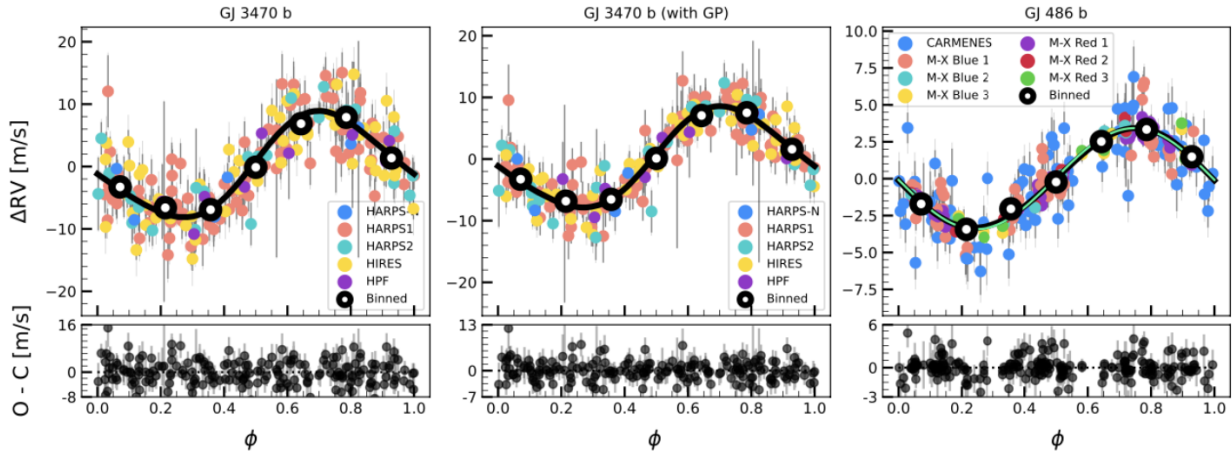


Fig. C.3. Phase-folded radial velocity curves for the transiting planets (fragment).

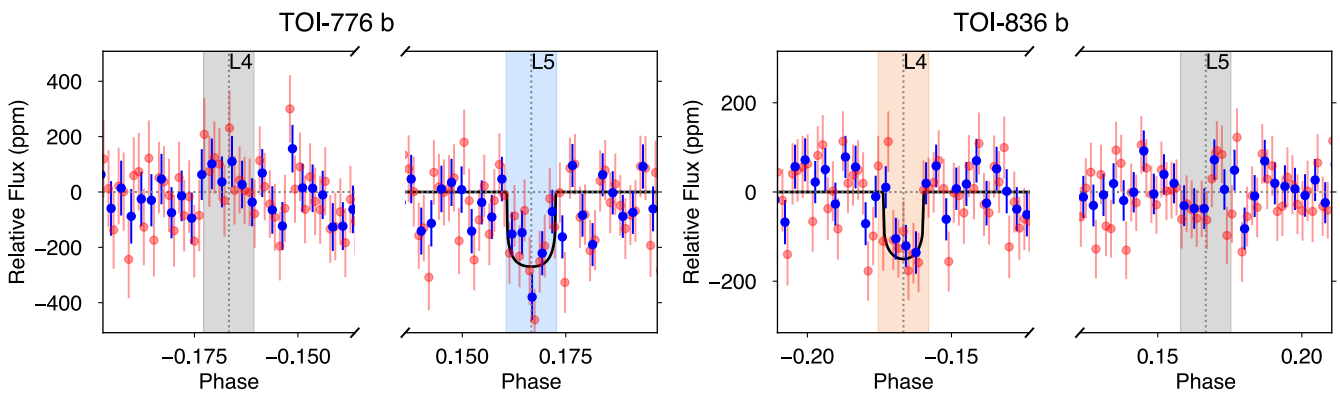


Fig. C.4. Phase-folded light curves around the L_4 and L_5 regions for the WC sample (fragment).

⁵ <https://zenodo.org/records/12636623>